An asymptotic preserving scheme for the two-dimensional shallow water equations with Coriolis forces

Xin Liu [a], Alina Chertock [b,*], Alexander Kurganov [a,c]

[a] *Department of Mathematics, Southern University of Science and Technology, Shenzhen, 518055, China*
[b] *Department of Mathematics, North Carolina State University, Raleigh, NC 27695, USA*
[c] *Mathematics Department, Tulane University, New Orleans, LA 70118, USA*

A R T I C L E   I N F O

A B S T R A C T

We consider the two-dimensional Saint-Venant system of shallow water equations with Coriolis forces. We focus on the case of a low Froude number, in which the system is stiff and conventional explicit numerical methods are extremely inefficient and often impractical. Our goal is to design an asymptotic preserving (AP) scheme, which is uniformly asymptotically consistent and stable for a broad range of (low) Froude numbers. The goal is achieved using the flux splitting proposed in [Haack et al., Commun. Comput. Phys., 12 (2012), pp. 955–980] in the context of isentropic Euler and Navier-Stokes equations. We split the flux into the stiff and nonstiff parts and then use an implicit-explicit approach: apply an explicit hyperbolic solver (we use the second-order central-upwind scheme) to the nonstiff part of the system while treating the stiff part of it implicitly. Moreover, the stiff part of the flux is linear and therefore we reduce the implicit stage of the proposed method to solving a Poisson-type elliptic equation, which is discretized using a standard second-order central difference scheme.

We conduct a series of numerical experiments, which demonstrate that the developed AP scheme achieves the theoretical second-order rate of convergence and the time-step stability restriction is independent of the Froude number. This makes the proposed AP scheme an efficient and robust alternative to fully explicit numerical methods.

1. Introduction

We consider the two-dimensional (2-D) Saint-Venant system of shallow water equations with Coriolis forces:

$$h_t + (hu)_x + (hv)_y = 0, \tag{1.1}$$

$$(hu)_t + \left(hu^2 + \frac{g}{2}h^2\right)_x + (huv)_y = fhv, \tag{1.2}$$

$$(hv)_t + (huv)_x + \left(hv^2 + \frac{g}{2}h^2\right)_y = -fhu, \tag{1.3}$$

where t is the time, x and y are horizontal spatial coordinates, $h(x, y, t)$ is the water depth, $u(x, y, t)$ and $v(x, y, t)$ are the x- and y-components of the flow velocity, g is the constant gravitational acceleration, and f is the Coriolis parameter.

---

* Corresponding author.
   E-mail addresses: xliu111@uottawa.ca (X. Liu), chertock@math.ncsu.edu (A. Chertock), kurganov@math.tulane.edu (A. Kurganov).

The system (1.1)–(1.3) is often used to model atmospheric and oceanic flows. In such large scale phenomena, Froude number is used to describe different flow regimes and, as discussed in [22], low Froude numbers give rise to multiple spatial or temporal scales or both. Low Froude numbers are typically observed in many physics, engineering and industrial phenomena, for example, as described in [4], the reference Froude number is around 0.03 in the atmospheric and oceanic flows. We note that the zero Froude number limit solution is challenging due to the following two major reasons. First, the type of the Saint-Venant system changes from hyperbolic to mixed hyperbolic-elliptic. Second, the system becomes very stiff, which makes it extremely difficult to design efficient and accurate methods for its numerical solution. For example, if conventional explicit schemes are used, then the spatial mesh size is supposed to be proportional to the Froude number and the time-step size, restricted by the CFL condition, is supposed to be even smaller as the propagation speeds of the system (1.1)–(1.3) are inversely proportional to the Froude number; see, e.g., [12,13,30]. This may lead to very expensive computational cost when numerically solving the Saint-Venant system with Coriolis forces in the low Froude number regime.

In order to overcome the aforementioned difficulties, a class of algorithms named asymptotic preserving (AP) schemes have been developed and recently attracted a lot of attentions. According to definition in [17,18], an AP scheme gives a consistent and stable discretization of a continuous physical model for all values of a singular perturbation parameter (throughout the paper, we will denote this parameter by ε). In particular, the scheme is AP if it is uniformly stable in ε, that is, the stability time-step restriction is independent of ε.

The AP schemes have been widely studied for the kinetic equations; see, e.g., [16,19,20] and references therein. They have been also applied to the low Mach number compressible Euler and Navier-Stokes equations in [5,8–10,14,21,29]. Several AP schemes have been developed for the shallow water equations; see e.g., [4,11,33]. Adding Coriolis forces to the Saint Venant system brings another level of complexity since in this case, not only the hydrostatic pressure, but also the Coriolis term is stiff in the low Froude number regime. To the best of our knowledge, no AP scheme for the shallow water equations with Coriolis forces has been ever reported; we can only refer the reader to the recent paper [34], where an asymptotically consistent method has been developed for rotating shallow water equations with Coriolis forces.

In this paper, we develop an AP scheme for the shallow water equations with Coriolis forces. Our method is based on the hyperbolic flux splitting proposed in [14] in the context of isentropic Euler and Navier-Stokes equations. We split the flux into the stiff and nonstiff parts and then use an implicit-explicit approach: apply an explicit hyperbolic solver (we use the second-order central-upwind scheme developed in [25,26] for general multidimensional hyperbolic systems of conservation laws; also see [23,24]) to the nonstiff part of the system while treating the stiff part of it implicitly. Moreover, the stiff part of the flux is linear and therefore we reduce the implicit stage of the proposed method to solving a Poisson-type elliptic equation, which is discretized using a standard second-order central difference scheme.

The paper is organized as follows. In §2, we first rewrite the system (1.1)–(1.3) in a dimensionless form and explain the numerical difficulty for solving this system in the low Froude regime. In §3, we follow the flux splitting idea from [14] and develop an AP scheme for the shallow water equations with Coriolis forces. In §4, we verify the performance of the developed AP scheme on two numerical examples. Some concluding remarks complete the paper in §5.

2. Dimensional analysis

We first rewrite the Saint-Venant system with Coriolis forces (1.1)–(1.3) in the dimensionless form. To this end, we introduce the characteristic length ℓ_0, characteristic depth h_0, and characteristic velocity w_0. Therefore, the dimensionless variables can be defined by

$$\widehat{x} := \frac{x}{\ell_0}, \quad \widehat{y} := \frac{y}{\ell_0}, \quad \widehat{h} := \frac{h}{h_0}, \quad \widehat{u} := \frac{u}{w_0}, \quad \widehat{v} := \frac{v}{w_0}.$$

Substituting them into (1.1)–(1.3) and dropping the hats in the notations, we obtain the dimensionless form of the shallow water equations with Coriolis forces:

$$\text{Sr} \cdot h_t + (hu)_x + (hv)_y = 0, \tag{2.1}$$

$$\text{Sr} \cdot (hu)_t + \left(hu^2 + \frac{1}{\text{Fr}^2} \frac{h^2}{2} \right)_x + (huv)_y = \frac{1}{\text{Ro}} hv, \tag{2.2}$$

$$\text{Sr} \cdot (hv)_t + (huv)_x + \left(hv^2 + \frac{1}{\text{Fr}^2} \frac{h^2}{2} \right)_y = -\frac{1}{\text{Ro}} hu, \tag{2.3}$$

in which

$$\text{Sr} := \frac{\ell_0}{t_0 w_0}, \quad \text{Fr} := \frac{w_0}{\sqrt{gh_0}} \quad \text{and} \quad \text{Ro} = \frac{w_0}{\ell_0 f}$$

are the Strouhal, Froude and Rossby numbers, respectively. After choosing $t_0 = \ell_0/w_0$ and $h_0 = \ell_0^2/g$ and the reference Froude number $\text{Fr} = \varepsilon$, we obtain $\text{Sr} = 1$ and $\text{Ro} = \varepsilon$, and rewrite the system (2.1)–(2.3) as

$$h_t + (hu)_x + (hv)_y = 0, \tag{2.4}$$

$$(hu)_t + \left(hu^2 + \frac{1}{\varepsilon^2}\frac{h^2}{2}\right)_x + (huv)_y = \frac{1}{\varepsilon}hv, \tag{2.5}$$

$$(hv)_t + (huv)_x + \left(hv^2 + \frac{1}{\varepsilon^2}\frac{h^2}{2}\right)_y = -\frac{1}{\varepsilon}hu, \tag{2.6}$$

which is considered in a certain domain Ω, that is, for $(x, y) \in \Omega$.

In the vector form, the system (2.4)–(2.6) reads as

$$\boldsymbol{U}_t + \boldsymbol{F}(\boldsymbol{U})_x + \boldsymbol{G}(\boldsymbol{U})_y = \boldsymbol{S}(\boldsymbol{U}),$$

where $\boldsymbol{U} := (h, hu, hv)^\top$ is the vector of unknown quantities, $\boldsymbol{F}(\boldsymbol{U}) := \left(hu, hu^2 + h^2/(2\varepsilon^2), huv\right)^\top$ and $\boldsymbol{G}(\boldsymbol{U}) := \left(hv, huv, hv^2 + h^2/(2\varepsilon^2)\right)^\top$ are the x- and y-fluxes, and $\boldsymbol{S}(\boldsymbol{U}) := \left(0, hv/\varepsilon, -hu/\varepsilon\right)^\top$ is the source term due to Coriolis forces. The eigenvalues of the Jacobians $\partial \boldsymbol{F}/\partial \boldsymbol{U}$ and $\partial \boldsymbol{G}/\partial \boldsymbol{U}$ are

$$\left\{u \pm \frac{1}{\varepsilon}\sqrt{h},\, u\right\} \quad \text{and} \quad \left\{v \pm \frac{1}{\varepsilon}\sqrt{h},\, v\right\},$$

respectively. Therefore, if one discretizes the spatial domain Ω using Cartesian cells of size $\Delta x \Delta y$ and uses an explicit scheme to numerically solve the system (2.4)–(2.6), the CFL condition yields the following time-step restriction:

$$\Delta t_{\text{expl}} \leq \nu \cdot \min\left(\frac{\Delta x}{\max\limits_{u,h}\left\{|u| + \frac{1}{\varepsilon}\sqrt{h}\right\}},\, \frac{\Delta y}{\max\limits_{v,h}\left\{|v| + \frac{1}{\varepsilon}\sqrt{h}\right\}}\right) = \mathcal{O}(\varepsilon \Delta_{\min}), \tag{2.7}$$

where $\Delta_{\min} := \min(\Delta x, \Delta y)$ and $0 < \nu \leq 1$ is the CFL number. Moreover, numerical diffusion of explicit schemes would typically be proportional to $\varepsilon^{-1}\Delta_{\max}^p$, where $\Delta_{\max} := \max(\Delta x, \Delta y)$ and p is a formal order of the scheme, and thus one would have to choose $\Delta x = \mathcal{O}(\varepsilon^{1/p})$ and $\Delta y = \mathcal{O}(\varepsilon^{1/p})$ to prevent the numerical diffusion from dominating the solution. Hence, the stability restriction of time-step size would become $\Delta t = \mathcal{O}(\varepsilon^{1+1/p})$. This explains a significant computational cost of explicit schemes in the low Froude number regime.

3. An asymptotic preserving (AP) scheme

In this section, we develop an AP scheme for the shallow water system (2.4)–(2.6) and perform an asymptotic analysis to show that the scheme provides a consistent and stable discretization of the limiting system as the Froude number $\varepsilon \to 0$.

3.1. Analysis of the low Froude number limit

We first investigate the asymptotic limit of the shallow water equations (2.4)–(2.6) as $\varepsilon \to 0$. To this end, we substitute a formal asymptotic expansion

$$\boldsymbol{w} = \boldsymbol{w}^{(0)} + \varepsilon \boldsymbol{w}^{(1)} + \varepsilon^2 \boldsymbol{w}^{(2)} + \ldots \tag{3.1}$$

for the unknown variables $\boldsymbol{w} = (h, u, v)^\top$ into the system (2.4)–(2.6) and then collect the like powers of ε to obtain

$$\mathcal{O}(\varepsilon^{-2}): h^{(0)}h_x^{(0)} = 0,$$
$$h^{(0)}h_y^{(0)} = 0,$$
$$\mathcal{O}(\varepsilon^{-1}): h^{(0)}h_x^{(1)} + h^{(1)}h_x^{(0)} = h^{(0)}v^{(0)},$$
$$h^{(0)}h_y^{(1)} + h^{(1)}h_y^{(0)} = -h^{(0)}u^{(0)},$$
$$\mathcal{O}(1): h_t^{(0)} + (h^{(0)}u^{(0)})_x + (h^{(0)}v^{(0)})_y = 0,$$
$$(h^{(0)}u^{(0)})_t + \left[h^{(0)}(u^{(0)})^2\right]_x + \left(h^{(0)}h^{(2)}\right)_x + \left(h^{(0)}u^{(0)}v^{(0)}\right)_y + h^{(1)}h_x^{(1)}$$
$$= h^{(0)}v^{(1)} + h^{(1)}v^{(0)},$$
$$\left(h^{(0)}v^{(0)}\right)_t + \left[h^{(0)}(v^{(0)})^2\right]_y + \left(h^{(0)}h^{(2)}\right)_y + \left(h^{(0)}u^{(0)}v^{(0)}\right)_x + h^{(1)}h_y^{(1)}$$
$$= -h^{(0)}u^{(1)} - h^{(1)}u^{(0)},$$
$$\mathcal{O}(\varepsilon): h_t^{(1)} + (h^{(0)}u^{(1)})_x + (h^{(0)}v^{(1)})_y = 0, \tag{3.2}$$
$$\left(h^{(0)}u^{(1)} + h^{(1)}u^{(0)}\right)_t + 2\left(h^{(0)}u^{(0)}u^{(1)}\right)_x + \left[h^{(1)}(u^{(0)})^2\right]_x + \left(h^{(1)}h^{(2)}\right)_x$$
$$+ \left(h^{(0)}u^{(1)}v^{(0)}\right)_y + \left(h^{(1)}u^{(0)}v^{(0)}\right)_y + \left(h^{(0)}u^{(0)}v^{(1)}\right)_y$$
$$- h^{(1)}v^{(1)} - h^{(2)}v^{(0)} = h^{(0)}v^{(2)},$$
$$\left(h^{(0)}v^{(1)} + h^{(1)}v^{(0)}\right)_t + 2\left(h^{(0)}v^{(0)}v^{(1)}\right)_y + \left[h^{(1)}(v^{(0)})^2\right]_y + \left(h^{(1)}h^{(2)}\right)_y$$
$$+ \left(h^{(0)}u^{(1)}v^{(0)}\right)_x + \left(h^{(1)}u^{(0)}v^{(0)}\right)_x + \left(h^{(0)}u^{(0)}v^{(1)}\right)_x$$
$$+ h^{(1)}u^{(1)} + h^{(2)}u^{(0)} = -h^{(0)}u^{(2)},$$
$$\mathcal{O}(\varepsilon^2): h_t^{(2)} + \left(h^{(0)}u^{(2)}\right)_x + \left(h^{(0)}v^{(2)}\right)_y + \left(h^{(1)}u^{(1)}\right)_x + \left(h^{(1)}v^{(1)}\right)_y$$
$$+ \left(u^{(0)}h^{(2)}\right)_x + \left(v^{(0)}h^{(2)}\right)_y = 0.$$

The equations for the $\mathcal{O}(\varepsilon^{-2})$ terms in (3.2) imply

$$h_x^{(0)} = 0, \quad h_y^{(0)} = 0. \tag{3.3}$$

Substituting (3.3) into the continuity equation (2.4) and integrating it over the domain Ω yields

$$-(\ln h^{(0)})_t = \frac{1}{|\Omega|} \int_{\partial\Omega} \boldsymbol{\nabla} \cdot \boldsymbol{u}^{(0)},$$

where $\boldsymbol{u} := (u, v)^\top$. The last equation implies that $h^{(0)}$ is constant in both space and time, and the divergence-free condition $\boldsymbol{\nabla} \cdot \boldsymbol{u}^{(0)} = 0$ is satisfied for the leading order velocities $\boldsymbol{u}^{(0)}$ provided the system is considered subject to either periodic, reflecting (solid wall) or open boundary conditions. The equations for the $\mathcal{O}(1)$ terms in (3.2) yields

$$u^{(0)} = -h_y^{(1)}, \quad v^{(0)} = h_x^{(1)}, \tag{3.4}$$

which also imply that the leading order velocity field is divergence-free, that is,

$$u_x^{(0)} + v_y^{(0)} = 0. \tag{3.5}$$

We now differentiate the second and third $\mathcal{O}(1)$ equations in (3.2) with respect to y and x, receptively, and then substitute them into the first $\mathcal{O}(\varepsilon)$ equation to obtain

$$h_t^{(1)} - h^{(0)}\left(h_{xx}^{(1)} + h_{yy}^{(1)}\right)_t = h^{(0)}\left[(v^{(0)})^2 - (u^{(0)})^2\right]_{xy} + h^{(0)}\left[\left(u^{(0)}v^{(0)}\right)_{xx} - \left(u^{(0)}v^{(0)}\right)_{yy}\right]. \tag{3.6}$$

Similarly, we differentiate the second and third $\mathcal{O}(\varepsilon)$ equations in (3.2) with respect to y and x, receptively, substitute them into the $\mathcal{O}(\varepsilon^2)$ equation and then use (3.5) to obtain

$$h_t^{(2)} - \left(h^{(0)}v^{(1)} + h^{(1)}v^{(0)}\right)_{xt} + \left(h^{(0)}u^{(1)} + h^{(1)}u^{(0)}\right)_{yt} =$$
$$2h^{(0)}\left[v^{(0)}v^{(1)} - u^{(0)}u^{(1)}\right]_{xy} + \left[h^{(1)}\left((v^{(0)})^2 - (u^{(0)})^2\right)\right]_{xy} \tag{3.7}$$
$$+ \left(h^{(0)}u^{(1)}v^{(0)} + h^{(1)}u^{(0)}v^{(0)} + h^{(0)}u^{(0)}v^{(1)}\right)_{xx} - \left(h^{(0)}u^{(1)}v^{(0)} + h^{(1)}u^{(0)}v^{(0)} + h^{(0)}u^{(0)}v^{(1)}\right)_{yy}.$$

In summary, we use (3.3)–(3.7) and arrive at the following limiting equations:

$$h^{(0)} = \text{Const},$$
$$u_x^{(0)} + v_y^{(0)} = 0,$$
$$u^{(0)} = -h_y^{(1)},$$
$$v^{(0)} = h_x^{(1)},$$
$$(h^{(0)}u^{(0)})_t + \left[h^{(0)}(u^{(0)})^2 + \frac{1}{2}(h^{(1)})^2\right]_x + (h^{(0)}u^{(0)}v^{(0)})_y + h^{(0)}h_x^{(2)} = h^{(0)}v^{(1)} + h^{(1)}v^{(0)},$$
$$(h^{(0)}v^{(0)})_t + \left[h^{(0)}(v^{(0)})^2 + \frac{1}{2}(h^{(1)})^2\right]_y + (h^{(0)}u^{(0)}v^{(0)})_x + h^{(0)}h_y^{(2)} = -h^{(0)}u^{(1)} - h^{(1)}u^{(0)}, \tag{3.8}$$
$$h_t^{(1)} - h^{(0)}\left(h_{xx}^{(1)} + h_{yy}^{(1)}\right)_t = h^{(0)}\left[(v^{(0)})^2 - (u^{(0)})^2\right]_{xy} + h^{(0)}\left[\left(u^{(0)}v^{(0)}\right)_{xx} - \left(u^{(0)}v^{(0)}\right)_{yy}\right]$$
$$h_t^{(2)} - \left(h^{(0)}v^{(1)} + h^{(1)}v^{(0)}\right)_{xt} + \left(h^{(0)}u^{(1)} + h^{(1)}u^{(0)}\right)_{yt}$$
$$= 2h^{(0)}\left[v^{(0)}v^{(1)} - u^{(0)}u^{(1)}\right]_{xy} + \left[h^{(1)}\left((v^{(0)})^2 - (u^{(0)})^2\right)\right]_{xy}$$
$$+ \left(h^{(0)}u^{(1)}v^{(0)} + h^{(1)}u^{(0)}v^{(0)} + h^{(0)}u^{(0)}v^{(1)}\right)_{xx} - \left(h^{(0)}u^{(1)}v^{(0)} + h^{(1)}u^{(0)}v^{(0)} + h^{(0)}u^{(0)}v^{(1)}\right)_{yy}.$$

In the remaining part of §3, we develop an AP scheme for (2.4)–(2.6), which yields a consistent approximation of the limiting equations (3.8) as $\varepsilon \to 0$.

3.2. Hyperbolic flux splitting

In order to construct an AP scheme for the system (2.4)–(2.6), we follow the idea from [14] and split each of the fluxes into two parts corresponding to the slow and fast dynamics:

$$h_t + \alpha(hu)_x + \alpha(hv)_y + (1-\alpha)(hu)_x + (1-\alpha)(hv)_y = 0, \tag{3.9}$$

$$(hu)_t + \left(hu^2 + \frac{\frac{1}{2}h^2 - a(t)h}{\varepsilon^2}\right)_x + (huv)_y + \frac{a(t)}{\varepsilon^2}h_x = \frac{1}{\varepsilon}hv, \tag{3.10}$$

$$(hv)_t + (huv)_x + \left(hv^2 + \frac{\frac{1}{2}h^2 - a(t)h}{\varepsilon^2}\right)_y + \frac{a(t)}{\varepsilon^2}h_y = -\frac{1}{\varepsilon}hu. \tag{3.11}$$

This system can be written in the following vector form:

$$\boldsymbol{U}_t + \widetilde{\boldsymbol{F}}(\boldsymbol{U})_x + \widetilde{\boldsymbol{G}}(\boldsymbol{U})_y + \widehat{\boldsymbol{F}}(\boldsymbol{U})_x + \widehat{\boldsymbol{G}}(\boldsymbol{U})_y = \boldsymbol{S}(\boldsymbol{U}), \tag{3.12}$$

where the slow dynamics (nonstiff) parts of the fluxes $\widetilde{\boldsymbol{F}}$ and $\widetilde{\boldsymbol{G}}$ are

$$\widetilde{\boldsymbol{F}}(\boldsymbol{U}) := \begin{pmatrix} \alpha hu \\ hu^2 + \dfrac{\frac{1}{2}h^2 - a(t)h}{\varepsilon^2} \\ huv \end{pmatrix}, \quad \widetilde{\boldsymbol{G}}(\boldsymbol{U}) := \begin{pmatrix} \alpha hv \\ huv \\ hv^2 + \dfrac{\frac{1}{2}h^2 - a(t)h}{\varepsilon^2} \end{pmatrix} \tag{3.13}$$

and the fast dynamics (stiff) parts of the fluxes $\widehat{\boldsymbol{F}}$ and $\widehat{\boldsymbol{G}}$ and the source term $\boldsymbol{S}$ are

$$\widehat{\boldsymbol{F}}(\boldsymbol{U}) := \begin{pmatrix} (1-\alpha)hu \\ \dfrac{a(t)}{\varepsilon^2}h \\ 0 \end{pmatrix}, \quad \widehat{\boldsymbol{G}}(\boldsymbol{U}) := \begin{pmatrix} (1-\alpha)hv \\ 0 \\ \dfrac{a(t)}{\varepsilon^2}h \end{pmatrix}, \quad \boldsymbol{S}(\boldsymbol{U}) := \begin{pmatrix} 0 \\ \dfrac{1}{\varepsilon}hv \\ -\dfrac{1}{\varepsilon}hu \end{pmatrix}. \tag{3.14}$$

In order to ensure that the subsystem $\boldsymbol{U}_t + \widetilde{\boldsymbol{F}}(\boldsymbol{U})_x + \widetilde{\boldsymbol{G}}(\boldsymbol{U})_y = \boldsymbol{0}$ is both nonstiff and hyperbolic, we need to choose the flux splitting parameters α and $a(t)$ in an appropriate way. To this end, we first compute the eigenvalues of the Jacobians $\partial \widetilde{\boldsymbol{F}}/\partial \boldsymbol{U}$ and $\partial \widetilde{\boldsymbol{G}}/\partial \boldsymbol{U}$, which are

$$
\left\{ u \pm \sqrt{(1-\alpha)u^2 + \alpha \frac{h-a(t)}{\varepsilon^2}}, \, u \right\} \quad \text{and} \quad \left\{ v \pm \sqrt{(1-\alpha)v^2 + \alpha \frac{h-a(t)}{\varepsilon^2}}, \, v \right\}, \tag{3.15}
$$

respectively. We then take

$$
\alpha = \varepsilon^s \quad \text{and} \quad a(t) = \min_{(x,y)\in\Omega} h(x,y,t), \tag{3.16}
$$

where $s \geq 1$. Using the asymptotic expansion (3.1) for h and $a(t)$ and the fact that $h^{(0)}$ is constant over the entire domain Ω, we obtain $h - a(t) = \mathcal{O}(\varepsilon)$ and thus (3.16) guarantees that all of the eigenvalues in (3.15) are real and uniformly bounded with respect to ε.

Remark 3.1. Even though one can take any value of $s \geq 1$ in (3.16), it might be safer to take $s = 2$ there as in this case the stability time-step restriction, which is based on (3.15) and (3.16), will be clearly independent of ε. In the numerical experiments reported in §4, we have used $s = 2$, that is, $\alpha = \varepsilon^2$. However, the results obtained with $s = 1$ (not reported in this paper) are almost identical and no instabilities have been observed as expected.

3.3. Implicit-explicit (IMEX) time discretization

In order to relax the strong stability restriction on the time-step size, we follow the implicit-explicit approach and approximate the nonstiff flux terms $\widetilde{\boldsymbol{F}}(\boldsymbol{U})_x$ and $\widetilde{\boldsymbol{G}}(\boldsymbol{U})_y$ explicitly and stiff flux terms $\widehat{\boldsymbol{F}}(\boldsymbol{U})_x$ and $\widehat{\boldsymbol{G}}(\boldsymbol{U})_y$ as well as the Coriolis term $\boldsymbol{S}(\boldsymbol{U})$ implicitly.

Let us consider the simplest first-order IMEX method (the forward-backward Euler method from [1]) and apply it to discretize the system (3.9)–(3.11) in time. This results in

$$
\frac{h^{n+1} - h^n}{\Delta t} + \alpha(hu)^n_x + \alpha(hv)^n_y + (1-\alpha)(hu)^{n+1}_x + (1-\alpha)(hv)^{n+1}_y = 0, \tag{3.17}
$$

$$
\frac{(hu)^{n+1} - (hu)^n}{\Delta t} + \left(hu^2 + \frac{\frac{1}{2}h^2 - a^n h}{\varepsilon^2} \right)^n_x + (huv)^n_y + \frac{a^n}{\varepsilon^2} h^{n+1}_x = \frac{1}{\varepsilon}(hv)^{n+1}, \tag{3.18}
$$

$$
\frac{(hv)^{n+1} - (hv)^n}{\Delta t} + (huv)^n_x + \left(hv^2 + \frac{\frac{1}{2}h^2 - a^n h}{\varepsilon^2} \right)^n_y + \frac{a^n}{\varepsilon^2} h^{n+1}_y = -\frac{1}{\varepsilon}(hu)^{n+1}, \tag{3.19}
$$

where the upper indices n and $n+1$ corresponds to the current, t^n, and new, $t^{n+1} = t^n + \Delta t$, time levels, respectively. Notice that in the process of evolution of the solution from $t = t^n$ to $t = t^{n+1}$, we fix the splitting parameter $a(t) = a^n := a(t^n)$ as it must be computed using the available set of values of h at the current time level.

The remaining part of §3 is organized as follows. In §3.4, we describe the central-upwind spatial discretization of the nonstiff flux terms. In §3.5, we discretize the stiff flux and Coriolis terms using the central differences and implement a higher-order IMEX method to complete the derivation of the second-order AP scheme. In §3.6, we prove that the resulting fully discrete system is asymptotically consistent as $\varepsilon \to 0$.

3.4. Central-upwind discretization of the nonstiff flux terms

In order to discretize the studied system (3.12)–(3.14), we use a finite-volume approach. We divide the computational domain into finite-volume cells $C_{j,k} = (x_{j-\frac{1}{2}}, x_{j+\frac{1}{2}}) \times (y_{k-\frac{1}{2}}, y_{k+\frac{1}{2}})$, where $x_{j+\frac{1}{2}} - x_{j-\frac{1}{2}} \equiv \Delta x$ and $y_{k+\frac{1}{2}} - y_{k-\frac{1}{2}} \equiv \Delta y$, and assume that the solution at the current time level $t = t^n$ is available in terms of its cell averages:

$$
\overline{\boldsymbol{U}}^n_{j,k} \approx \frac{1}{\Delta x \Delta y} \iint_{C_{j,k}} \boldsymbol{U}(x,y,t^n) \, \mathrm{d}x\mathrm{d}y.
$$

In this section, we describe a finite-volume discretization of the nonstiff flux terms. In each cell, we approximate the contribution of $\boldsymbol{R} := -\widetilde{\boldsymbol{F}}(\boldsymbol{U})_x - \widetilde{\boldsymbol{G}}(\boldsymbol{U})_y$ by computing

$$
\mathcal{R}^n_{j,k} := -\frac{\widetilde{\mathcal{F}}^n_{j+\frac{1}{2},k} - \widetilde{\mathcal{F}}^n_{j-\frac{1}{2},k}}{\Delta x} - \frac{\widetilde{\mathcal{G}}^n_{j,k+\frac{1}{2}} - \widetilde{\mathcal{G}}^n_{j,k-\frac{1}{2}}}{\Delta y}, \tag{3.20}
$$

where $\widetilde{\mathcal{F}}$ and $\widetilde{\mathcal{G}}$ are the central-upwind fluxes from [25,26] (we note that a first-order version of the central upwind flux have been developed in [15]):

$$\widetilde{\mathcal{F}}^n_{j+\frac{1}{2},k} = \frac{a^+_{j+\frac{1}{2},k}\widetilde{\boldsymbol{F}}(\boldsymbol{U}^{\mathrm{E}}_{j,k}) - a^-_{j+\frac{1}{2},k}\widetilde{\boldsymbol{F}}(\boldsymbol{U}^{\mathrm{W}}_{j+1,k})}{a^+_{j+\frac{1}{2},k} - a^-_{j+\frac{1}{2},k}} + \frac{a^+_{j+\frac{1}{2},k}a^-_{j+\frac{1}{2},k}}{a^+_{j+\frac{1}{2},k} - a^-_{j+\frac{1}{2},k}}\left(\boldsymbol{U}^{\mathrm{W}}_{j+1,k} - \boldsymbol{U}^{\mathrm{E}}_{j,k}\right) \tag{3.21}$$

and

$$\widetilde{\mathcal{G}}^n_{j,k+\frac{1}{2}} = \frac{b^+_{j,k+\frac{1}{2}}\widetilde{\boldsymbol{G}}(\boldsymbol{U}^{\mathrm{N}}_{j,k}) - b^-_{j,k+\frac{1}{2}}\widetilde{\boldsymbol{G}}(\boldsymbol{U}^{\mathrm{S}}_{j,k+1})}{b^+_{j,k+\frac{1}{2}} - b^-_{j,k+\frac{1}{2}}} + \frac{b^+_{j,k+\frac{1}{2}}b^-_{j,k+\frac{1}{2}}}{b^+_{j,k+\frac{1}{2}} - b^-_{j,k+\frac{1}{2}}}\left(\boldsymbol{U}^{\mathrm{S}}_{j,k+1} - \boldsymbol{U}^{\mathrm{N}}_{j,k}\right). \tag{3.22}$$

Here, $\boldsymbol{U}^{\mathrm{E}}_{j,k}$, $\boldsymbol{U}^{\mathrm{W}}_{j,k}$, $\boldsymbol{U}^{\mathrm{N}}_{j,k}$ and $\boldsymbol{U}^{\mathrm{S}}_{j,k}$ are point values of $\boldsymbol{U}$ at time $t = t^n$ computed using a piecewise linear reconstruction. To minimize oscillations, we reconstruct the primitive quantities $\boldsymbol{w}$ rather than the conservative ones, $\boldsymbol{U}$. This is done in the following way. In each cell, we approximate the function $\boldsymbol{w}(x, y, t^n)$ using a linear piece

$$\widetilde{\boldsymbol{w}}(x, y)^n := \boldsymbol{w}^n_{j,k} + (\boldsymbol{w}_x)^n_{j,k}(x - x_j) + (\boldsymbol{w}_y)^n_{j,k}(y - y_k), \quad (x, y) \in C_{j,k}, \tag{3.23}$$

where $\boldsymbol{w}^n_{j,k} = (\overline{h}^n_{j,k}, u^n_{j,k}, v^n_{j,k})^\top$, $u^n_{j,k} = \overline{(hu)}^n_{j,k}/\overline{h}^n_{j,k}$, $v^n_{j,k} = \overline{(hv)}^n_{j,k}/\overline{h}^n_{j,k}$, and the slopes $\boldsymbol{w}_x$ and $\boldsymbol{w}_y$ are computed in a non-oscillatory manner using a nonlinear limiter. In the numerical results reported in §4 below, we have used the generalized minmod limiter (see, e.g., [27,28,31,32]):

$$(\boldsymbol{w}_x)^n_{j,k} = \mathrm{minmod}\left(\theta\frac{\boldsymbol{w}^n_{j+1,k} - \boldsymbol{w}^n_{j,k}}{\Delta x}, \frac{\boldsymbol{w}^n_{j+1,k} - \boldsymbol{w}^n_{j-1,k}}{2\Delta x}, \theta\frac{\boldsymbol{w}^n_{j,k} - \boldsymbol{w}^n_{j-1,k}}{\Delta x}\right),$$
$$(\boldsymbol{w}_y)^n_{j,k} = \mathrm{minmod}\left(\theta\frac{\boldsymbol{w}^n_{j,k+1} - \boldsymbol{w}^n_{j,k}}{\Delta y}, \frac{\boldsymbol{w}^n_{j,k+1} - \boldsymbol{w}^n_{j,k-1}}{2\Delta y}, \theta\frac{\boldsymbol{w}^n_{j,k} - \boldsymbol{w}^n_{j,k-1}}{\Delta y}\right), \tag{3.24}$$

with the minmod function

$$\mathrm{minmod}(z_1, z_2, \cdots) := \begin{cases} \min(z_1, z_2, \cdots), & \text{if } z_i > 0 \ \forall i, \\ \max(z_1, z_2, \cdots), & \text{if } z_i < 0 \ \forall i, \\ 0, & \text{otherwise}, \end{cases} \tag{3.25}$$

which is applied in a componentwise manner. The parameter $\theta \in [1, 2]$ controls the amount of numerical dissipation: the larger the θ, the smaller the numerical dissipation. In the numerical results reported in §4 below, we have taken $\theta = 2$.

Finally, the one-sided local speeds of propagation $a^\pm_{j+\frac{1}{2},k}$ and $b^\pm_{j,k+\frac{1}{2}}$ in the x- and y-directions, respectively, are estimated at time $t = t^n$ from the smallest and largest eigenvalues of the Jacobians $\partial\widetilde{\boldsymbol{F}}/\partial\boldsymbol{U}$ and $\partial\widetilde{\boldsymbol{G}}/\partial\boldsymbol{U}$:

$$a^+_{j+\frac{1}{2},k} = \max\left(u^{\mathrm{E}}_{j,k} + \sqrt{(1-\alpha)(u^{\mathrm{E}}_{j,k})^2 + \alpha\frac{h^{\mathrm{E}}_{j,k} - a^n}{\varepsilon^2}}, u^{\mathrm{W}}_{j+1,k} + \sqrt{(1-\alpha)(u^{\mathrm{W}}_{j+1,k})^2 + \alpha\frac{h^{\mathrm{W}}_{j+1,k} - a^n}{\varepsilon^2}}, 0\right),$$
$$a^-_{j+\frac{1}{2},k} = \min\left(u^{\mathrm{E}}_{j,k} - \sqrt{(1-\alpha)(u^{\mathrm{E}}_{j,k})^2 + \alpha\frac{h^{\mathrm{E}}_{j,k} - a^n}{\varepsilon^2}}, u^{\mathrm{W}}_{j+1,k} - \sqrt{(1-\alpha)(u^{\mathrm{W}}_{j+1,k})^2 + \alpha\frac{h^{\mathrm{W}}_{j+1,k} - a^n}{\varepsilon^2}}, 0\right),$$
$$b^+_{j,k+\frac{1}{2}} = \max\left(v^{\mathrm{N}}_{j,k} + \sqrt{(1-\alpha)(v^{\mathrm{N}}_{j,k})^2 + \alpha\frac{h^{\mathrm{N}}_{j,k} - a^n}{\varepsilon^2}}, v^{\mathrm{S}}_{j,k+1} + \sqrt{(1-\alpha)(v^{\mathrm{S}}_{j,k+1})^2 + \alpha\frac{h^{\mathrm{S}}_{j,k+1} - a^n}{\varepsilon^2}}, 0\right),$$
$$b^-_{j,k+\frac{1}{2}} = \min\left(v^{\mathrm{N}}_{j,k} - \sqrt{(1-\alpha)(v^{\mathrm{N}}_{j,k})^2 + \alpha\frac{h^{\mathrm{N}}_{j,k} - a^n}{\varepsilon^2}}, v^{\mathrm{S}}_{j,k+1} - \sqrt{(1-\alpha)(v^{\mathrm{S}}_{j,k+1})^2 + \alpha\frac{h^{\mathrm{S}}_{j,k+1} - a^n}{\varepsilon^2}}, 0\right). \tag{3.26}$$

3.4.1. Numerical diffusion of the central-upwind discretization (3.20)–(3.26)

In this section, we analyze the leading order of the numerical diffusion present at the central-upwind discretization (3.20)–(3.26). To this end, we first rewrite the x-directional central-upwind flux (3.21) as

$$\widetilde{\mathcal{F}}^n_{j+\frac{1}{2},k} = \frac{\widetilde{\boldsymbol{F}}(\overline{\boldsymbol{U}}^n_{j,k}) + \widetilde{\boldsymbol{F}}(\overline{\boldsymbol{U}}^n_{j+1,k})}{2} + \mathcal{D}^n_{j+\frac{1}{2},k}, \tag{3.27}$$

where

$$
\begin{aligned}
\mathcal{D}^n_{j+\frac{1}{2},k} ={}& \frac{a^+_{j+\frac{1}{2},k}}{2(a^+_{j+\frac{1}{2},k} - a^-_{j+\frac{1}{2},k})} \Big[2\widetilde{\boldsymbol{F}}(\boldsymbol{U}^{\mathrm{E}}_{j,k}) - \widetilde{\boldsymbol{F}}(\overline{\boldsymbol{U}}^n_{j,k}) - \widetilde{\boldsymbol{F}}(\overline{\boldsymbol{U}}^n_{j+1,k}) \Big] \\
& - \frac{a^-_{j+\frac{1}{2},k}}{2(a^+_{j+\frac{1}{2},k} - a^-_{j+\frac{1}{2},k})} \Big[2\widetilde{\boldsymbol{F}}(\boldsymbol{U}^{\mathrm{W}}_{j+1,k}) - \widetilde{\boldsymbol{F}}(\overline{\boldsymbol{U}}^n_{j,k}) - \widetilde{\boldsymbol{F}}(\overline{\boldsymbol{U}}^n_{j+1,k}) \Big] \\
& + \frac{a^+_{j+\frac{1}{2},k} a^-_{j+\frac{1}{2},k}}{a^+_{j+\frac{1}{2},k} - a^-_{j+\frac{1}{2},k}} \left(\boldsymbol{U}^{\mathrm{W}}_{j+1,k} - \boldsymbol{U}^{\mathrm{E}}_{j,k} \right),
\end{aligned}
\tag{3.28}
$$

represent the numerical diffusion introduced by the central-upwind discretization and all of the point values and local speeds of propagation in (3.28) are computed at time level $t = t^n$ as indicated in the previous section. In what follows we introduce the notation $\boldsymbol{\mathcal{D}} := (\mathcal{D}^h, \mathcal{D}^{hu}, \mathcal{D}^{hv})^\top$ to specify the components of the diffusion.

We now compute the leading order of the numerical diffusion in (3.28). We consider the following asymptotic expansion for the unknowns in (3.28):

$$
\begin{aligned}
\overline{\boldsymbol{w}}^n_{j,k} &= \boldsymbol{w}^{(0),n}_{j,k} + \varepsilon \boldsymbol{w}^{(1),n}_{j,k} + \varepsilon^2 \boldsymbol{w}^{(2),n}_{j,k} + \dots, \\
\boldsymbol{w}^{\mathrm{E}}_{j,k} &= \boldsymbol{w}^{\mathrm{E},(0)}_{j,k} + \varepsilon \boldsymbol{w}^{\mathrm{E},(1)}_{j,k} + \varepsilon^2 \boldsymbol{w}^{\mathrm{E},(2)}_{j,k} + \dots, \\
\boldsymbol{w}^{\mathrm{W}}_{j,k} &= \boldsymbol{w}^{\mathrm{W},(0)}_{j,k} + \varepsilon \boldsymbol{w}^{\mathrm{W},(1)}_{j,k} + \varepsilon^2 \boldsymbol{w}^{\mathrm{W},(2)}_{j,k} + \dots.
\end{aligned}
$$

We assume that $h^{(0),n}_{j,k} = h^{(0),n}$ for all j,k, where $h^{(0),n} = \mathrm{Const}$, and all the limiting equations (3.8) are satisfied at time level t^n. Thus, (3.23)–(3.25) imply $h^{\mathrm{E},(0)}_{j,k} = h^{\mathrm{W},(0)}_{j,k} = h^{(0),n}$. Moreover, using the definition of a^n in (3.16), we can expand

$$
a^n = h^{(0),n} + \varepsilon a^{(1),n} + \varepsilon^2 a^{(2),n} + \dots,
$$

where $a^{(1),n}$ and $a^{(2),n}$ are constants at time t^n.

For the first component of the numerical diffusion in (3.28), we obtain

$$
\begin{aligned}
\mathcal{D}^{h,n}_{j+\frac{1}{2},k} ={}& \frac{\alpha\, a^+_{j+\frac{1}{2},k}}{2(a^+_{j+\frac{1}{2},k} - a^-_{j+\frac{1}{2},k})} \Big[2h^{\mathrm{E},(0)}_{j,k} u^{\mathrm{E},(0)}_{j,k} - h^{(0),n}_{j,k} u^{(0),n}_{j,k} - h^{(0),n}_{j+1,k} u^{(0),n}_{j+1,k} \Big] \\
& - \frac{\alpha\, a^-_{j+\frac{1}{2},k}}{2(a^+_{j+\frac{1}{2},k} - a^-_{j+\frac{1}{2},k})} \Big[2h^{\mathrm{W},(0)}_{j+1,k} u^{\mathrm{W},(0)}_{j+1,k} - h^{(0),n}_{j,k} u^{(0),n}_{j,k} - h^{(0),n}_{j+1,k} u^{(0),n}_{j+1,k} \Big] \\
& + \frac{\varepsilon\, a^+_{j+\frac{1}{2},k} a^-_{j+\frac{1}{2},k}}{a^+_{j+\frac{1}{2},k} - a^-_{j+\frac{1}{2},k}} \left(h^{\mathrm{W},(1)}_{j+1,k} - h^{\mathrm{E},(1)}_{j,k} \right)
\end{aligned}
\tag{3.29}
$$

for the leading order approximation. Since we take $\alpha = \varepsilon^s$ where $s \geq 1$ (see §3.2), the leading order of $\mathcal{D}^{h,n}_{j+\frac{1}{2},k}$ in (3.29) is $\mathcal{O}(\varepsilon)$.

For the second component of the numerical diffusion in (3.27), we obtain

$$
\begin{aligned}
\mathcal{D}^{hu,n}_{j+\frac{1}{2},k} ={}& \frac{a^+_{j+\frac{1}{2},k}}{2(a^+_{j+\frac{1}{2},k} - a^-_{j+\frac{1}{2},k})} \left\{ \frac{1}{2\varepsilon^2} \Big[(h^{(0),n}_{j,k})^2 + (h^{(0),n}_{j+1,k})^2 - 2(h^{\mathrm{E},(0)}_{j,k})^2 \Big] \right. \\
& \left. + \frac{a^{(1),n}}{\varepsilon} \Big[h^{(0),n}_{j,k} + h^{(0),n}_{j+1,k} - 2h^{\mathrm{E},(0)}_{j,k} \Big] \right\} \\
& - \frac{a^-_{j+\frac{1}{2},k}}{2(a^+_{j+\frac{1}{2},k} - a^-_{j+\frac{1}{2},k})} \left\{ \frac{1}{2\varepsilon^2} \Big[(h^{(0),n}_{j,k})^2 + (h^{(0),n}_{j+1,k})^2 - 2(h^{\mathrm{W},(0)}_{j+1,k})^2 \Big] \right. \\
& \left. + \frac{a^{(1),n}}{\varepsilon} \Big[h^{(0),n}_{j,k} + h^{(0),n}_{j+1,k} - 2h^{\mathrm{W},(0)}_{j+1,k} \Big] \right\} \\
& + \frac{a^+_{j+\frac{1}{2},k} a^-_{j+\frac{1}{2},k}}{a^+_{j+\frac{1}{2},k} - a^-_{j+\frac{1}{2},k}} \left(h^{\mathrm{W},(0)}_{j+1,k} u^{\mathrm{W},(0)}_{j+1,k} - h^{\mathrm{E},(0)}_{j,k} u^{\mathrm{E},(0)}_{j,k} \right),
\end{aligned}
\tag{3.30}
$$

in which all of the $\mathcal{O}(\varepsilon^{-2})$ and $\mathcal{O}(\varepsilon^{-1})$ terms can be canceled since $h_{j,k}^{E,(0)} = h_{j,k}^{W,(0)} = h_{j,k}^{(0),n} = h^{(0),n}$ for all j, k. Therefore, the leading order of $\mathcal{D}_{j+\frac{1}{2},k}^{hu,n}$ in (3.30) is $\mathcal{O}(1)$.

For the third component of the numerical diffusion in (3.27), we have

$$
\begin{aligned}
\mathcal{D}_{j+\frac{1}{2},k}^{hv,n} &= \frac{a_{j+\frac{1}{2},k}^+}{2(a_{j+\frac{1}{2},k}^+ - a_{j+\frac{1}{2},k}^-)} \left[2h_{j,k}^{E,(0)} u_{j,k}^{E,(0)} v_{j,k}^{E,(0)} - h_{j,k}^{(0),n} u_{j,k}^{(0),n} v_{j,k}^{(0),n} - h_{j+1,k}^{(0),n} u_{j+1,k}^{(0),n} v_{j+1,k}^{(0),n} \right] \\
&\quad - \frac{a_{j+\frac{1}{2},k}^-}{2(a_{j+\frac{1}{2},k}^+ - a_{j+\frac{1}{2},k}^-)} \left[2h_{j+1,k}^{W,(0)} u_{j+1,k}^{W,(0)} v_{j+1,k}^{W,(0)} - h_{j,k}^{(0),n} u_{j,k}^{(0),n} v_{j,k}^{(0),n} - h_{j+1,k}^{(0),n} u_{j+1,k}^{(0),n} v_{j+1,k}^{(0),n} \right] \\
&\quad + \frac{a_{j+\frac{1}{2},k}^+ a_{j+\frac{1}{2},k}^-}{a_{j+\frac{1}{2},k}^+ - a_{j+\frac{1}{2},k}^-} \left(h_{j+1,k}^{W,(0)} v_{j+1,k}^{W,(0)} - h_{j,k}^{E,(0)} v_{j,k}^{E,(0)} \right)
\end{aligned}
\tag{3.31}
$$

for the leading order approximation. Therefore, the leading order of $\mathcal{D}_{j+\frac{1}{2},k}^{hv,n}$ in (3.31) is $\mathcal{O}(1)$.

Similarly, for the y-directional central-upwind flux (3.22), we obtain that the leading orders of the numerical diffusion is $\mathcal{O}(\varepsilon)$, $\mathcal{O}(1)$ and $\mathcal{O}(1)$ for the first, second and third components, respectively.

Finally, substituting the x- and y-directional central-upwind fluxes into (3.20), we obtain

$$
\mathcal{R}_{j,k}^n := -D_x \widetilde{\boldsymbol{F}}_{j,k}^n - D_y \widetilde{\boldsymbol{G}}_{j,k}^n + \mathcal{Q}_{j,k}^n,
\tag{3.32}
$$

where

$$
D_x \zeta_{j,k} := \frac{\zeta_{j+1,k} - \zeta_{j-1,k}}{2\Delta x} \quad \text{and} \quad D_y \zeta_{j,k} := \frac{\zeta_{j,k+1} - \zeta_{j,k-1}}{2\Delta y}
$$

are discrete central difference operators and $\mathcal{Q}_{j,k}^n := (\mathcal{Q}_{j,k}^{h,n}, \mathcal{Q}_{j,k}^{hu,n}, \mathcal{Q}_{j,k}^{hv,n})^\top$ is a numerical diffusion, which can be expanded with respect to ε in the following way:

$$
\begin{aligned}
\mathcal{Q}_{j,k}^{h,n} &= \varepsilon \mathcal{Q}_{j,k}^{h,(1),n} + \varepsilon^2 \mathcal{Q}_{j,k}^{h,(2),n} + \varepsilon^3 \mathcal{Q}_{j,k}^{h,(3),n} + \dots, \\
\mathcal{Q}_{j,k}^{hu,n} &= \mathcal{Q}_{j,k}^{hu,(0),n} + \varepsilon \mathcal{Q}_{j,k}^{hu,(1),n} + \varepsilon^2 \mathcal{Q}_{j,k}^{hu,(2),n} + \dots, \\
\mathcal{Q}_{j,k}^{hv,n} &= \mathcal{Q}_{j,k}^{hv,(0),n} + \varepsilon \mathcal{Q}_{j,k}^{hv,(1),n} + \varepsilon^2 \mathcal{Q}_{j,k}^{hv,(2),n} + \dots.
\end{aligned}
\tag{3.33}
$$

We would like to stress that all of the terms in this expansion are proportional to $\Delta_{\max}^2$ since they are introduced by the second-order central-upwind discretization.

3.5. Fully discrete AP schemes

In order to derive a fully discrete AP scheme, we first rewrite the system (3.17)–(3.19) by using the notation $\boldsymbol{R}^n := (R^{h,n}, R^{hu,n}, R^{hv,n})^\top$ and solving (3.17) for h^{n+1} and (3.18), (3.19) for $(hu)^{n+1}$ and $(hv)^{n+1}$:

$$
h^{n+1} = h^n + \Delta t R^{h,n} - \Delta t(1-\alpha) \left[(hu)_x^{n+1} + (hv)_y^{n+1} \right],
\tag{3.34}
$$

$$
(hu)^{n+1} = \frac{1}{K} \left[(hu)^n + \frac{\Delta t}{\varepsilon}(hv)^n + \Delta t \left(R^{hu,n} + \frac{\Delta t}{\varepsilon} R^{hv,n} \right) - \frac{a^n \Delta t}{\varepsilon^2} \left(h_x^{n+1} + \frac{\Delta t}{\varepsilon} h_y^{n+1} \right) \right],
\tag{3.35}
$$

$$
(hv)^{n+1} = \frac{1}{K} \left[(hv)^n - \frac{\Delta t}{\varepsilon}(hu)^n + \Delta t \left(R^{hv,n} - \frac{\Delta t}{\varepsilon} R^{hu,n} \right) - \frac{a^n \Delta t}{\varepsilon^2} \left(h_y^{n+1} - \frac{\Delta t}{\varepsilon} h_x^{n+1} \right) \right],
\tag{3.36}
$$

where

$$
K := 1 + (\Delta t/\varepsilon)^2.
\tag{3.37}
$$

We then follow [9] and differentiate equations (3.35) and (3.36) with respect to x and y, respectively, substitute them into equation (3.34) and obtain the following elliptic equation for h^{n+1}:

$$
\begin{aligned}
h^{n+1} - \frac{a^n(1-\alpha)}{\widetilde{K}} \left(h_{xx}^{n+1} + h_{yy}^{n+1} \right) &= h^n + \Delta t R^{h,n} - \frac{\Delta t(1-\alpha)}{K} \Bigg[(hu)_x^n + (hv)_y^n \\
&\quad + \frac{\Delta t}{\varepsilon} \left((hv)_x^n - (hu)_y^n \right) + \Delta t \left(R_x^{hu,n} + R_y^{hv,n} \right) + \frac{(\Delta t)^2}{\varepsilon} \left(R_x^{hv,n} - R_y^{hu,n} \right) \Bigg],
\end{aligned}
\tag{3.38}
$$

where

$$\widetilde{K} := 1 + (\varepsilon/\Delta t)^2. \tag{3.39}$$

Next, we construct a fully discrete method for (3.9)–(3.11) by numerically solving the elliptic equation (3.38) for h^{n+1} and using its solution in equations (3.35) and (3.36) to obtain $(hu)^{n+1}$ and $(hv)^{n+1}$. To this end, we compute the nonstiff flux terms $R^{h,n}$, $R^{hu,n}$ and $R^{hv,n}$ using the central-upwind flux approximation from §3.4 and discretize all of the spatial derivatives in (3.38) using the standard second-order central differences. This results in

$$\overline{h}_{j,k}^{n+1} - \frac{a^n(1-\alpha)}{\widetilde{K}}\Delta \overline{h}_{j,k}^{n+1} = \overline{h}_{j,k}^n + \Delta t \mathcal{R}_{j,k}^{h,n}$$
$$- \frac{\Delta t(1-\alpha)}{K}\left[D_x\overline{(hu)}_{j,k}^n + D_y\overline{(hv)}_{j,k}^n + \frac{\Delta t}{\varepsilon}\left(D_x\overline{(hv)}_{j,k}^n - D_y\overline{(hu)}_{j,k}^n \right)\right. \tag{3.40}$$
$$\left. + \Delta t\left(D_x\mathcal{R}_{j,k}^{hu,n} + D_y\mathcal{R}_{j,k}^{hv,n}\right) + \frac{(\Delta t)^2}{\varepsilon}\left(D_x\mathcal{R}_{j,k}^{hv,n} - D_y\mathcal{R}_{j,k}^{hu,n}\right)\right],$$

where $\boldsymbol{\mathcal{R}}_{j,k}^n = (\mathcal{R}_{j,k}^{h,n}, \mathcal{R}_{j,k}^{hu,n}, \mathcal{R}_{j,k}^{hv,n})^\top$ is defined in (3.20)–(3.22) and we use the following notation for the discrete Laplacian:

$$\Delta\zeta_{j,k} := \frac{\zeta_{j+1,k} - 2\zeta_{j,k} + \zeta_{j-1,k}}{(\Delta x)^2} + \frac{\zeta_{j,k+1} - 2\zeta_{j,k} + \zeta_{j,k-1}}{(\Delta y)^2}.$$

After solving the linear algebra system (3.40) for $\{\overline{h}_{j,k}^{n+1}\}$, we substitute it into equations (3.35) and (3.36) discretized using the standard central differences and end up with

$$\overline{(hu)}_{j,k}^{n+1} = \frac{1}{K}\left[\overline{(hu)}_{j,k}^n + \frac{\Delta t}{\varepsilon}\overline{(hv)}_{j,k}^n + \Delta t\left(\mathcal{R}_{j,k}^{hu,n} + \frac{\Delta t}{\varepsilon}\mathcal{R}_{j,k}^{hv,n}\right)\right.$$
$$\left. - \frac{a^n\Delta t}{\varepsilon^2}\left(D_x\overline{h}_{j,k}^{n+1} + \frac{\Delta t}{\varepsilon}D_y\overline{h}_{j,k}^{n+1}\right)\right], \tag{3.41}$$

$$\overline{(hv)}_{j,k}^{n+1} = \frac{1}{K}\left[\overline{(hv)}_{j,k}^n - \frac{\Delta t}{\varepsilon}\overline{(hu)}_{j,k}^n + \Delta t\left(\mathcal{R}_{j,k}^{hv,n} - \frac{\Delta t}{\varepsilon}\mathcal{R}_{j,k}^{hu,n}\right)\right.$$
$$\left. - \frac{a^n\Delta t}{\varepsilon^2}\left(D_y\overline{h}_{j,k}^{n+1} - \frac{\Delta t}{\varepsilon}D_x\overline{h}_{j,k}^{n+1}\right)\right]. \tag{3.42}$$

Notice that the scheme (3.40)–(3.42) is second-order accurate in space, but only first-order accurate in time. In order to increase a temporal order of accuracy to the second one, we implement a two-stage globally stiffly accurate IMEX Runge-Kutta scheme ARS(2,2,2), which can be described by the following Butcher tableau:

$$\begin{array}{c|ccc||ccc}
0 & 0 & 0 & 0 & 0 & 0 & 0 \\
\gamma & \gamma & 0 & 0 & 0 & \gamma & 0 \\
1 & 1-\frac{1}{2\gamma} & \frac{1}{2\gamma} & 0 & 0 & 1-\gamma & \gamma \\
\hline
& 1-\frac{1}{2\gamma} & \frac{1}{2\gamma} & 0 & 0 & 1-\gamma & \gamma
\end{array} \tag{3.43}$$

where $\gamma = 1 - 1/\sqrt{2}$; see [1]. Details on the implementation of the ARS(2,2,2) method are provided in Appendix A.

3.5.1. Numerical diffusion and stability of the proposed AP scheme

It should be observed that the numerical diffusion present in the proposed fully discrete AP scheme is introduced by the explicit central-upwind discretization $\mathcal{R}_{j,k}^n$. Recall that the diffusion terms $\varepsilon\Delta_{\max}^2$, $\Delta_{\max}^2$ and $\Delta_{\max}^2$, respectively, and their influence on the numerical solution (3.40)–(3.42) computed at the new time level is small. Indeed, the largest contribution of the numerical diffusion will be introduced by the terms proportional to $\mathcal{Q}_{j,k}^{h,n}$, $\frac{1}{K\varepsilon}\mathcal{Q}_{j,k}^{hu,n}$ and $\frac{1}{K\varepsilon}\mathcal{Q}_{j,k}^{hv,n}$, which are $\mathcal{O}(\varepsilon)$ since the coefficient K defined in (3.37) is proportional to ε^{-2}. We therefore conclude that unlike the case of explicit schemes discussed at the end of §2, the proposed second-order AP scheme is uniformly stable and accurate in ε.

The stability of the designed AP scheme will be guaranteed by [14, Lemma 3.1], as both the slow dynamic (nonstiff) and fast dynamic (stiff) parts of the studied system are discretized in a stable manner. Since the fast dynamic part is treated implicitly, the stability of the proposed AP scheme is controlled by the CFL condition for the slow dynamic part, which using the eigenvalues given by (3.15), can be written as follows (compare with (2.7)):

$$\Delta t_{\text{AP}} \leq \nu \cdot \min\left(\frac{\Delta x}{\max\limits_{u,h}\left\{|u| + \sqrt{(1-\alpha)u^2 + \alpha\frac{h-a(t)}{\varepsilon^2}}\right\}}, \frac{\Delta y}{\max\limits_{v,h}\left\{|v| + \sqrt{(1-\alpha)v^2 + \alpha\frac{h-a(t)}{\varepsilon^2}}\right\}} \right). \tag{3.44}$$

As it has been explained at the end of §3.2, the denominators on the right-hand side (RHS) of the previous equation are independent of ε (provided α is selected as in (3.16)). Therefore, the use of large time steps of size $\Delta t_{AP} = \mathcal{O}(\Delta_{\min})$, will be sufficient to enforce the stability of the proposed AP scheme.

3.6. The discrete low Froude number limit

In this section, we prove the AP property of the fully discrete scheme (3.40)–(3.42). To this end, we consider the following asymptotic expansions for the unknowns

$$
\begin{aligned}
\overline{h}^n_{j,k} &= h^{(0),n}_{j,k} + \varepsilon h^{(1),n}_{j,k} + \varepsilon^2 h^{(2),n}_{j,k} + \dots, \\
u^n_{j,k} &= u^{(0),n}_{j,k} + \varepsilon u^{(1),n}_{j,k} + \varepsilon^2 u^{(2),n}_{j,k} + \dots, \\
v^n_{j,k} &= v^{(0),n}_{j,k} + \varepsilon v^{(1),n}_{j,k} + \varepsilon^2 v^{(2),n}_{j,k} + \dots, \\
a^n &= h^{(0),n} + \varepsilon a^{(1),n} + \varepsilon^2 a^{(2),n} + \dots,
\end{aligned}
\tag{3.45}
$$

and assume that the discrete analogs of the first four equations in (3.8) are satisfied at time level $t = t^n$. Namely,

$$
h^{(0),n}_{j,k} = h^{(0),n}, \quad D_x u^{(0),n}_{j,k} + D_y v^{(0),n}_{j,k} = 0, \quad v^{(0),n}_{j,k} = D_x h^{(1),n}_{j,k}, \quad u^{(0),n}_{j,k} = -D_y h^{(1),n}_{j,k}, \quad \forall j,k.
\tag{3.46}
$$

We then formally expand the solution at time level $t = t^{n+1}$ with respect to ε:

$$
\begin{aligned}
\overline{h}^{n+1}_{j,k} &= h^{(0),n+1}_{j,k} + \varepsilon h^{(1),n+1}_{j,k} + \varepsilon^2 h^{(2),n+1}_{j,k} + \dots, \\
u^{n+1}_{j,k} &= u^{(0),n+1}_{j,k} + \varepsilon u^{(1),n+1}_{j,k} + \varepsilon^2 u^{(2),n+1}_{j,k} + \dots, \\
v^{n+1}_{j,k} &= v^{(0),n+1}_{j,k} + \varepsilon v^{(1),n+1}_{j,k} + \varepsilon^2 v^{(2),n+1}_{j,k} + \dots.
\end{aligned}
\tag{3.47}
$$

This expansion can be justified as follows. We first notice that subtracting $h^{(0),n}$ from both sides of (3.40) and taking into account (3.32) and (3.46) yield

$$
\left[I - \frac{a^n(1-\alpha)}{\widetilde{K}} \Delta \right] (\overline{h}^{n+1}_{j,k} - h^{(0),n}) = \mathcal{O}(\varepsilon),
\tag{3.48}
$$

where $a^n(1-\alpha)/\widetilde{K} = h^{(0),n} + \mathcal{O}(\varepsilon)$. Since the matrix $I - \frac{a^n(1-\alpha)}{K}\Delta$ is positive definite and non-singular (with eigenvalues bounded away from zero independently of ε), equation (3.48) implies

$$
\overline{h}^{n+1}_{j,k} = h^{(0),n} + \mathcal{O}(\varepsilon).
\tag{3.49}
$$

It follows from (3.41) and (3.42) that $\overline{(hu)}^{n+1}_{j,k} = \mathcal{O}(1)$ and $\overline{(hv)}^{n+1}_{j,k} = \mathcal{O}(1)$, which together with (3.49) gives

$$
u^{n+1}_{j,k} = u^{(0),n+1}_{j,k} + \mathcal{O}(\varepsilon) \quad \text{and} \quad v^{n+1}_{j,k} = v^{(0),n+1}_{j,k} + \mathcal{O}(\varepsilon).
$$

Next, we substitute (3.32), (3.33) and (3.45)–(3.47) into (3.40)–(3.42), which are for convenience multiplied by $\widetilde{K}$ defined by (3.39), to show that the fully discrete scheme provides a consistent approximation of the limiting system (3.8) as $\varepsilon \to 0$.

We first look at how the terms balance at each order in ε as $\varepsilon \to 0$. For the $\mathcal{O}(\varepsilon^{-1})$ terms appearing in (3.41) and (3.42), we take into account (3.46) to obtain

$$
D_x h^{(0),n+1}_{j,k} \equiv 0, \quad D_y h^{(0),n+1}_{j,k} \equiv 0,
$$

which indicates that $h^{(0),n+1}_{j,k}$ is constant in space, that is,

$$
h^{(0),n+1}_{j,k} \equiv h^{(0),n+1} = \text{Const}.
\tag{3.50}
$$

For the $\mathcal{O}(1)$ terms, we take into account (3.46) and (3.50) to obtain

$$
h^{(0),n+1} = h^{(0),n}, \quad u^{(0),n+1}_{j,k} = -D_y h^{(1),n+1}_{j,k}, \quad v^{(0),n+1}_{j,k} = D_x h^{(1),n+1}_{j,k}, \quad \forall j,k.
\tag{3.51}
$$

Remark 3.2. The first equation in (3.51) implies that the leading order water depth is constant not only in space but also in time, that is, $h^{(0),n+1} = h^{(0),n+1} = h^{(0)}$.

Remark 3.3. Taking central differences of the second and third equations in (3.51) with respect to y and x, respectively, we obtain

$$D_y v^{(0),n+1}_{j,k} + D_x u^{(0),n+1}_{j,k} = D_x D_y h^{(1),n+1}_{j,k} - D_y D_x h^{(1),n+1}_{j,k} = 0, \tag{3.52}$$

which implies that the divergence-free condition for the discrete velocity holds at all time levels.

Remark 3.4. It should be observed that the proposed AP scheme is also asymptotically well-balanced in the sense that it preserves geostrophic equilibria in the zero Froude number limit at the discrete level. Indeed, it is well-known that at the geostrophic equilibria, the pressure terms and Coriolis forces are balanced (see, e.g., [2,3,6,7,35]), which for the system (2.4)–(2.6) implies

$$u = -\frac{1}{\varepsilon} h_y, \quad v = \frac{1}{\varepsilon} h_x. \tag{3.53}$$

Substituting the expansions in (3.1) into (3.53) yields

$$u^{(0)} = -h^{(1)}_y, \quad v^{(0)} = h^{(1)}_x, \tag{3.54}$$

which are, in fact, the third and fourth equation in (3.8). We note that the second and third equations in (3.51), which have been obtained from the above discrete asymptotic analysis are consistent approximations of (3.54).

Next, we turn to the $\mathcal{O}(\varepsilon)$ terms. Using (3.46), (3.50), (3.51) and the fact that $\alpha = \varepsilon^s$, $s \geq 1$, the corresponding terms in equation (3.40) are

$$
\begin{aligned}
\frac{h^{(1),n+1}_{j,k} - h^{(1),n}_{j,k}}{\Delta t} - h^{(0)} \frac{\Delta h^{(1),n+1}_{j,k} - \Delta h^{(1),n}_{j,k}}{\Delta t} &= h^{(0)} D_x D_y \left[(v^{(0),n}_{j,k})^2 - (u^{(0),n}_{j,k})^2 \right] \\
&+ h^{(0)} \left[D_x^2 (u^{(0),n}_{j,k} v^{(0),n}_{j,k}) - D_y^2 (u^{(0),n}_{j,k} v^{(0),n}_{j,k}) \right] + \mathcal{Q}^{h,(1),n}_{j,k} + D_y \mathcal{Q}^{hu,(0),n}_{j,k} - D_x \mathcal{Q}^{hv,(0),n}_{j,k}.
\end{aligned} \tag{3.55}
$$

As one can easily see, this equation is a consistent discretization of (3.6) since the last three term on the RHS of (3.55) are $\mathcal{O}(\Delta^2_{\max})$ diffusion expansion coefficients from (3.33). We then use (3.46), (3.50) and (3.51) to obtain that the $\mathcal{O}(\varepsilon)$ terms in (3.41) and (3.42) are

$$
\begin{aligned}
\frac{h^{(0)} v^{(0),n+1}_{j,k} - h^{(0)} v^{(0),n}_{j,k}}{\Delta t} &+ D_y \left[h^{(0)} (v^{(0),n}_{j,k})^2 + \frac{1}{2} (h^{(1),n}_{j,k})^2 \right] + D_x \left(h^{(0)} u^{(0),n}_{j,k} v^{(0),n}_{j,k} \right) + h^{(0)} D_y \left(h^{(2),n+1}_{j,k} \right) \\
&= -h^{(0)} u^{(1),n+1}_{j,k} - h^{(1),n+1}_{j,k} u^{(0),n+1}_{j,k} + \mathcal{Q}^{hv,(0),n}_{j,k} + a^{(1),n} \left(u^{(0),n+1}_{j,k} - u^{(0),n}_{j,k} \right)
\end{aligned} \tag{3.56}
$$

and

$$
\begin{aligned}
\frac{h^{(0)} u^{(0),n+1}_{j,k} - h^{(0)} u^{(0),n}_{j,k}}{\Delta t} &+ D_x \left[h^{(0)} (u^{(0),n}_{j,k})^2 + \frac{1}{2} (h^{(1),n}_{j,k})^2 \right] + D_y \left(h^{(0)} u^{(0),n}_{j,k} v^{(0),n}_{j,k} \right) + h^{(0)} D_x \left(h^{(2),n+1}_{j,k} \right) \\
&= h^{(0)} v^{(1),n+1}_{j,k} + h^{(1),n+1}_{j,k} v^{(0),n+1}_{j,k} + \mathcal{Q}^{hu,(0),n}_{j,k} - a^{(1),n} \left(v^{(0),n+1}_{j,k} - v^{(0),n}_{j,k} \right),
\end{aligned} \tag{3.57}
$$

respectively. We note that equations (3.57) and (3.56) are consistent discretizations of the fourth and fifth equations in (3.8), respectively, since the last two term on the RHSs of (3.56) and (3.57) represent the numerical diffusion: while $\mathcal{Q}^{hv,(0),n}_{j,k}$ and $\mathcal{Q}^{hu,(0),n}_{j,k}$ are $\mathcal{O}(\Delta^2_{\max})$ diffusion expansion coefficients from (3.33), the terms $a^{(1),n} \left(u^{(0),n+1}_{j,k} - u^{(0),n}_{j,k} \right)$ and $-a^{(1),n} \left(v^{(0),n+1}_{j,k} - v^{(0),n}_{j,k} \right)$ are temporal diffusion terms proportional to $\mathcal{O}(\Delta t)$.

Finally, we derive the equation for $h^{(2),n+1}_{j,k}$ by considering the $\mathcal{O}(\varepsilon^2)$ terms in equation (3.40). To this end, we first take $\alpha = \varepsilon^2$ in (3.16) (we note that this value of α has been used in the numerical experiments reported in §4) and use (3.46), (3.50) and (3.51) to obtain

$$
\begin{aligned}
\frac{h_{j,k}^{(2),n+1} - h_{j,k}^{(2),n}}{\Delta t} &- \frac{1}{\Delta t} \Bigg\{ D_x^2 \left[h^{(0)} (u_{j,k}^{(0),n})^2 \right] + D_y^2 \left[h^{(0)} (v_{j,k}^{(0),n})^2 \right] + \frac{1}{2} \Delta \left[(h_{j,k}^{(1),n})^2 \right] \\
&+ 2 D_x D_y \left(h^{(0)} u_{j,k}^{(0),n} v_{j,k}^{(0),n} \right) + h^{(0)} \Delta h_{j,k}^{(2),n+1} \\
&- D_x \left(h^{(0)} v_{j,k}^{(1),n} + h_{j,k}^{(1),n} v_{j,k}^{(0),n} \right) + D_y \left(h^{(0)} u_{j,k}^{(1),n} + h_{j,k}^{(1),n} u_{j,k}^{(0),n} \right) \\
&+ a^{(1),n} \left[\Delta h_{j,k}^{(1),n+1} - \Delta h_{j,k}^{(1),n} \right] - D_x \mathcal{Q}_{j,k}^{hu,(0),n} - D_y \mathcal{Q}_{j,k}^{hv,(0),n} \Bigg\} \\
&= 2 h^{(0)} D_x D_y \left(v_{j,k}^{(0),n} v_{j,k}^{(1),n} - u_{j,k}^{(0),n} u_{j,k}^{(1),n} \right) + D_x D_y \left[h_{j,k}^{(1),n} \left((v_{j,k}^{(0),n})^2 - (u_{j,k}^{(0),n})^2 \right) \right] \\
&+ D_x^2 \left(h^{(0)} u_{j,k}^{(1),n} v_{j,k}^{(0),n} + h_{j,k}^{(1),n} u_{j,k}^{(0),n} v_{j,k}^{(0),n} + h^{(0)} u_{j,k}^{(1),n} v_{j,k}^{(0),n} \right) \\
&- D_y^2 \left(h^{(0)} u_{j,k}^{(1),n} v_{j,k}^{(0),n} + h_{j,k}^{(1),n} u_{j,k}^{(0),n} v_{j,k}^{(0),n} + h^{(0)} u_{j,k}^{(1),n} v_{j,k}^{(0),n} \right) \\
&+ \mathcal{Q}_{j,k}^{h,(2),n} + D_y \mathcal{Q}_{j,k}^{hu,(1),n} - D_x \mathcal{Q}_{j,k}^{hv,(1),n}.
\end{aligned}
\tag{3.58}
$$

We then apply the D_y and D_x operators to (3.56) and (3.57), respectively, add the resulting equations, and use (3.46) and (3.51) to obtain

$$
\begin{aligned}
D_x^2 \left[h^{(0)} (u_{j,k}^{(0),n})^2 \right] &+ D_y^2 \left[h^{(0)} (v_{j,k}^{(0),n})^2 \right] + \frac{1}{2} \Delta \left[(h_{j,k}^{(1),n})^2 \right] + 2 D_x D_y \left(h^{(0)} u_{j,k}^{(0),n} v_{j,k}^{(0),n} \right) + h^{(0)} \Delta h_{j,k}^{(2),n+1} \\
&= D_x \left(h^{(0)} v_{j,k}^{(1),n+1} + h_{j,k}^{(1),n+1} v_{j,k}^{(0),n+1} \right) - D_y \left(h^{(0)} u_{j,k}^{(1),n+1} + h_{j,k}^{(1),n+1} u_{j,k}^{(0),n+1} \right) \\
&- a^{(1),n} \left[\Delta h_{j,k}^{(1),n+1} - \Delta h_{j,k}^{(1),n} \right] + D_x \mathcal{Q}_{j,k}^{hu,(0),n} + D_y \mathcal{Q}_{j,k}^{hv,(0),n}.
\end{aligned}
\tag{3.59}
$$

Finally, we substitute (3.59) into (3.58) and end up with

$$
\begin{aligned}
\frac{h_{j,k}^{(2),n+1} - h_{j,k}^{(2),n}}{\Delta t} &- \frac{D_x \left(h^{(0)} v_{j,k}^{(1),n+1} + h_{j,k}^{(1),n+1} v_{j,k}^{(0),n+1} \right) - D_x \left(h^{(0)} v_{j,k}^{(1),n} + h_{j,k}^{(1),n} v_{j,k}^{(0),n} \right)}{\Delta t} \\
&+ \frac{D_y \left(h^{(0)} u_{j,k}^{(1),n+1} + h_{j,k}^{(1),n+1} u_{j,k}^{(0),n+1} \right) - D_y \left(h^{(0)} u_{j,k}^{(1),n} + h_{j,k}^{(1),n} u_{j,k}^{(0),n} \right)}{\Delta t} \\
&= 2 h^{(0)} D_x D_y \left(v_{j,k}^{(0),n} v_{j,k}^{(1),n} - u_{j,k}^{(0),n} u_{j,k}^{(1),n} \right) + D_x D_y \left[h_{j,k}^{(1),n} \left((v_{j,k}^{(0),n})^2 - (u_{j,k}^{(0),n})^2 \right) \right] \\
&+ D_x^2 \left(h^{(0)} u_{j,k}^{(1),n} v_{j,k}^{(0),n} + h_{j,k}^{(1),n} u_{j,k}^{(0),n} v_{j,k}^{(0),n} + h^{(0)} u_{j,k}^{(1),n} v_{j,k}^{(0),n} \right) \\
&- D_y^2 \left(h^{(0)} u_{j,k}^{(1),n} v_{j,k}^{(0),n} + h_{j,k}^{(1),n} u_{j,k}^{(0),n} v_{j,k}^{(0),n} + h^{(0)} u_{j,k}^{(1),n} v_{j,k}^{(0),n} \right) \\
&+ \mathcal{Q}_{j,k}^{h,(2),n} + D_y \mathcal{Q}_{j,k}^{hu,(1),n} - D_x \mathcal{Q}_{j,k}^{hv,(1),n}.
\end{aligned}
\tag{3.60}
$$

As one can see, this equation is a consistent discretization of (3.7) since the last three term on the RHS of (3.60) are $\mathcal{O}(\Delta_{\max}^2)$ diffusion expansion coefficients from (3.33).

In summary, the proposed numerical scheme yields the discrete limiting equations (3.50)–(3.52), (3.55)–(3.57) and (3.60), which are consistent approximations of the limiting system (3.8) as $\varepsilon \to 0$.

4. Numerical examples

In this section, we verify the efficiency and accuracy of the proposed AP scheme on two numerical examples.

Example 1—stationary vortex

In the first test problem, which was originally proposed in [2] and then slightly modified in [7], we consider a stationary vortex in the square domain $[-1, 1] \times [-1, 1]$ with a reflecting (solid wall) boundary condition in both x- and y-directions. We take the following initial conditions:
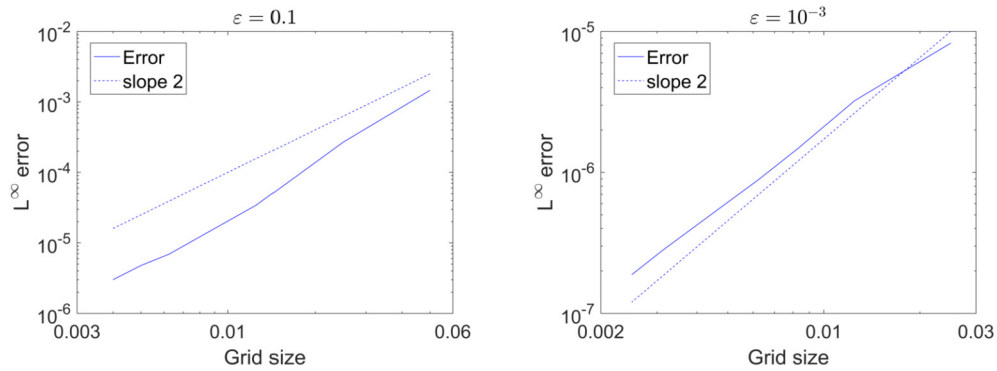
Fig. 1. Example 1: L^∞-errors for h computed using the AP scheme on several different grids for $\varepsilon = 0.1$ (left) and 10^{-3} (right).
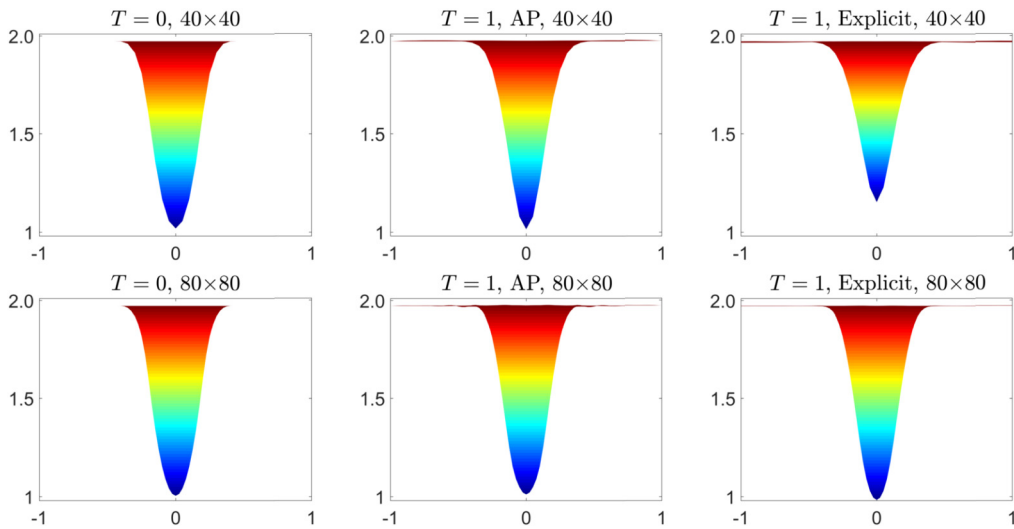
Fig. 2. Example 1: Side view of h computed by the AP and explicit schemes for $\varepsilon = 1$ using 40×40 (top row) and 80×80 (bottom row) grids.

$$h(r,0) = 1 + \varepsilon^2 \begin{cases} \dfrac{5}{2}(1 + 5\varepsilon^2)r^2, & r \leq \dfrac{1}{5}, \\[2mm] \dfrac{1}{10}(1 + 5\varepsilon^2) + 2r - \dfrac{3}{10} - \dfrac{5}{2}r^2 + \varepsilon^2\Big[4\ln(5r) + \dfrac{7}{2} - 20r + \dfrac{25}{2}r^2\Big], & \dfrac{1}{5} < r \leq \dfrac{2}{5}, \\[2mm] \dfrac{1}{5}(1 - 10\varepsilon^2 + 20\varepsilon^2\ln 2), & r \geq \dfrac{2}{5}. \end{cases}$$

$$u(x,y,0) = -\varepsilon y \Upsilon(r), \quad v(x,y,0) = \varepsilon x \Upsilon(r), \quad \Upsilon(r) := \begin{cases} 5, & r \leq \dfrac{1}{5}, \\[2mm] \dfrac{2}{r} - 5, & \dfrac{1}{5} < r \leq \dfrac{2}{5}, \\[2mm] 0, & r \geq \dfrac{2}{5}, \end{cases}$$

where $r := \sqrt{x^2 + y^2}$.

We first verify the order of convergence of the proposed AP scheme in the low Froude number regime. To this end, we compute the solution until the final time $T = 20$ for $\varepsilon = 0.01$ and 10^{-3} on several different grids with $\Delta x = \Delta y$. In Fig. 1, we plot the L^∞-errors in h as a function of the grid size together with a dashed line with slope=2 in the log-log scale. The obtained results confirm the experimental second order of convergence.

We then compare the results obtained by the proposed AP scheme with those computed by the explicit second-order semi-discrete central-upwind scheme from [7]. For both schemes, we select the time steps adaptively using the corresponding CFL conditions (3.44) and (2.7), respectively, with the CFL number $\nu = 0.2$. We use different uniform grids and compute the solutions until the final time $T = 1$.

We begin with the large Froude number $\varepsilon = 1$, for which the time-steps for both schemes are about the same. We show the obtained results (side view on the water depth h) in Fig. 2, where one can see that if a coarse 40×40 mesh is used, the
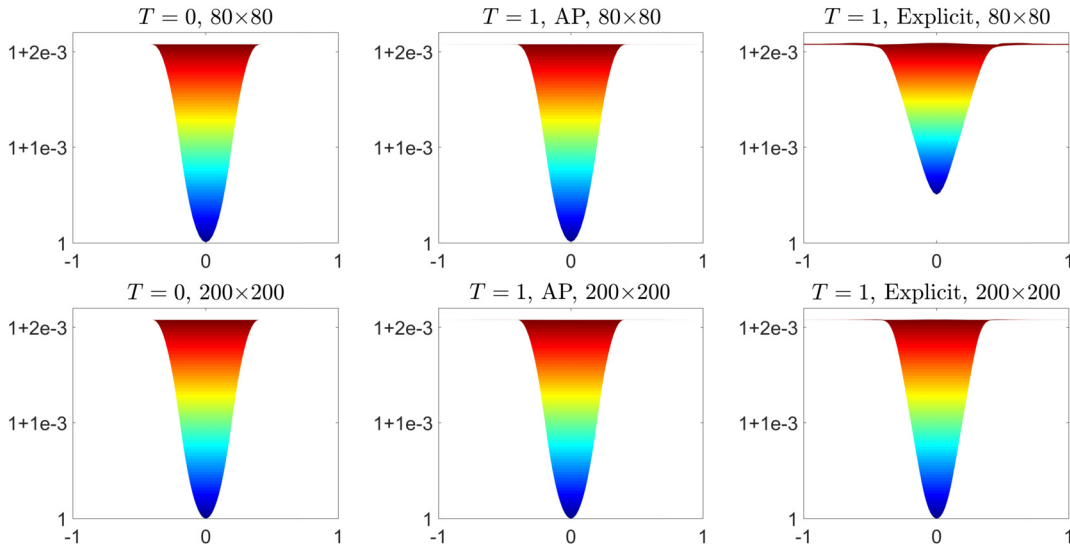
Fig. 3. Example 1: Side view of h computed by the AP and explicit schemes for $\varepsilon = 0.1$ using 80×80 (top row) and 200×200 (bottom row) grids.
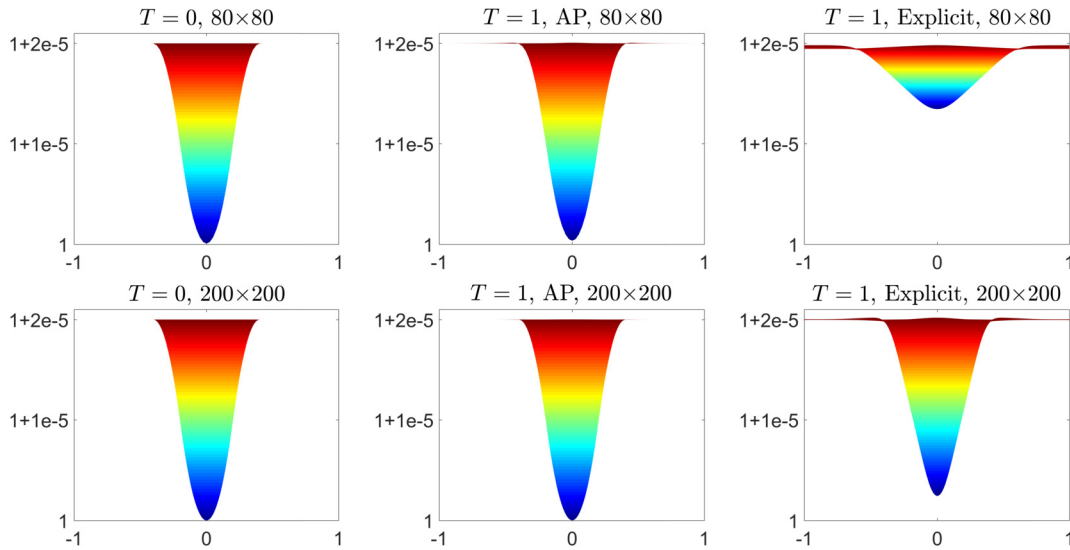
Fig. 4. Example 1: Side view of h computed by the AP and explicit schemes for $\varepsilon = 0.01$ using 80×80 (top row) and 200×200 (bottom row) grids.

AP scheme preserves the initial steady state much better than its explicit counterpart. When the mesh is refined to 80×80 cells, the obtained results are quite similar.

For a smaller Froude number $\varepsilon = 0.1$, the time-steps used by the AP scheme are already substantially larger than for the explicit scheme. Moreover, when we use the 80×80 grid, the resolution achieved by the AP scheme is much better; see the top row in Fig. 3. When the mesh is refined to 200×200 cells, the obtained results are quite similar (see the bottom row in Fig. 3), but the AP scheme is more efficient.

The difference between the proposed AP scheme and explicit one is pronounced even more for $\varepsilon = 0.01$, as one can see in Fig. 4. Note that on the 80×80 grid, the explicit scheme is very inaccurate since in this case Δx and Δy are not proportional to ε (see the dimensional analysis in §2), but even on the 200×200 grid the AP scheme clearly outperforms the explicit one.

It is also instructive to compare the CPU times consumed by both the AP and explicit schemes. We provide them in Table 1, where one can clearly observe huge computational savings for the AP scheme in the low Froude regime.

Finally, we consider regimes with very low Froude numbers $\varepsilon \leq 10^{-3}$. In such cases, explicit schemes are extremely computationally expensive and therefore we only show the results obtained by the developed AP schemes. In Fig. 5, we plot h computed by the AP for $\varepsilon = 10^{-3}$ (top row) and $\varepsilon = 10^{-4}$ (bottom row) at different times using the 200×200 uniform grid. As one can see, while the solution at a smaller time ($T = 10$) is quite accurate, at later times the numerical diffusion

Table 1
Example 1: CPU times consumed by the AP and explicit schemes on different grids for different values of ε. The final time is $T = 1$.

Grid	$\varepsilon = 1$		$\varepsilon = 0.1$		$\varepsilon = 0.01$	
	AP	Explicit	AP	Explicit	AP	Explicit
40×40	0.18 s	0.16 s	0.06 s	1.25 s	0.03 s	10.53 s
80×80	1.57 s	1.32 s	0.29 s	4.73 s	0.18 s	47.0 s
200×200	24.11 s	21.36 s	5.36 s	163.36 s	3.37 s	804.15 s
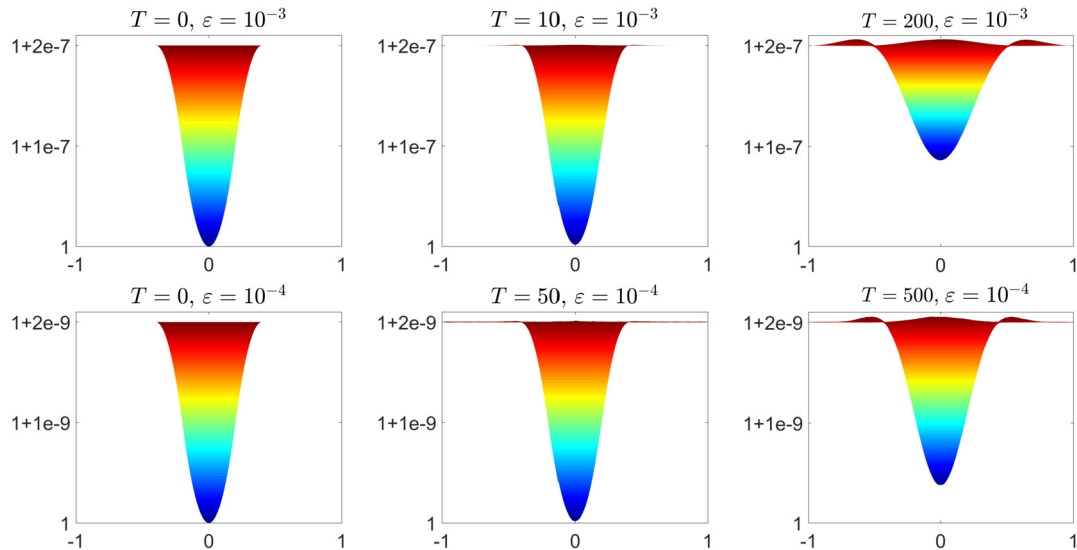
Fig. 5. Example 1: Side view of h computed by the AP scheme for $\varepsilon = 10^{-3}$ (top row) and $\varepsilon = 10^{-4}$ (bottom row) at different times using the 200×200 grid.
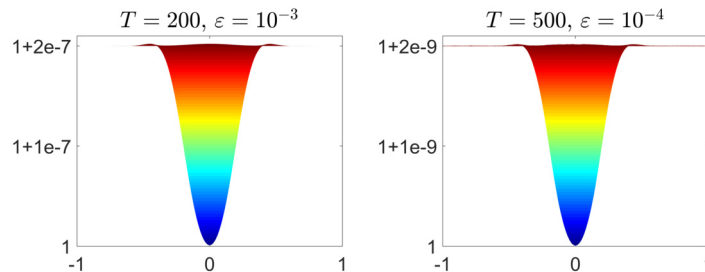
Fig. 6. Example 1: Side view of h computed by the AP scheme for $\varepsilon = 10^{-3}$ (left) and $\varepsilon = 10^{-4}$ (right) using the 500×500 grid.

present in the developed AP scheme starts dominating. We stress that for these very small values of ε the magnitude of the vortex is very small and it is hard to expect the vortex shape to be accurately preserved for long time using a relatively coarse grid. We therefore refine the mesh to 500×500 cells and compute the solutions for $\varepsilon = 10^{-3}$ and 10^{-4} at large times $T = 200$ and 500, respectively. The obtained results shown in Fig. 6, clearly demonstrate that even when for very small ε the AP scheme can achieve high resolution in a very efficient way: for $\varepsilon = 10^{-3}$ it requires only 422 time steps to evolve the solution until the final time $T = 200$ and for $\varepsilon = 10^{-4}$ it requires only 120 time steps to obtain the solution at time $T = 500$.

Example 2—traveling vortex

In this example, we take $\varepsilon = 10^{-2}$ and simulate a traveling vortex with the same initial water depth profile as in Example 1 in the same square domain $[-1, 1] \times [-1, 1]$ using a 100×100 uniform mesh and an open boundary condition in both the x- and y-directions. The initial velocities from Example 1 are now modified by adding a constant velocity vector $(15, 15)^\top$, namely, we take
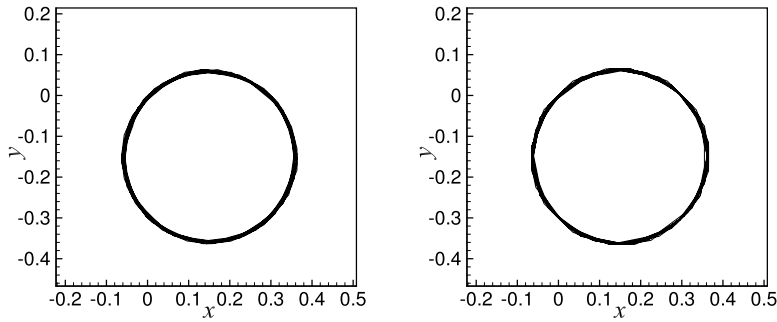
Fig. 7. Example 2: Trajectories of the traveling vortex center computed by the proposed AP (left) and explicit (right) schemes at times $0 \leq t \leq 0.98$.
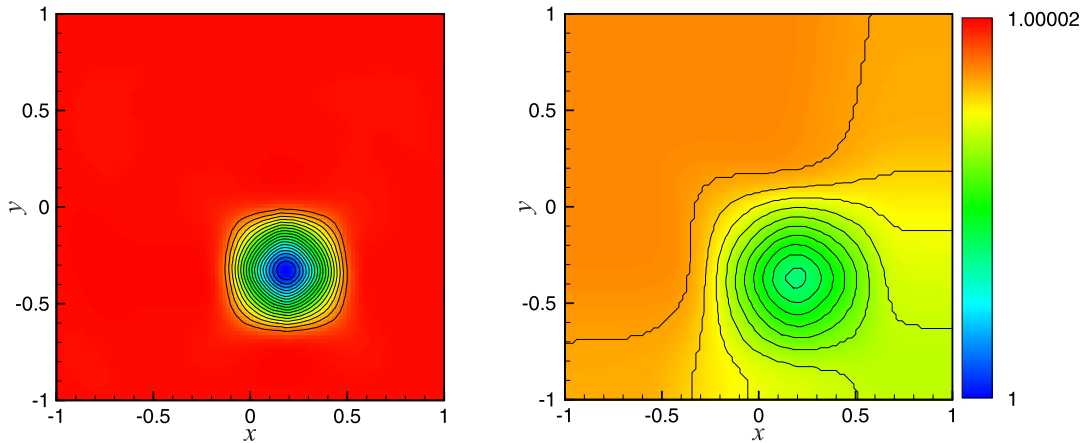
Fig. 8. Example 2: Contour lines of h computed by the proposed AP (left) and explicit (right) schemes.

$$u(x, y, 0) = 15 - \varepsilon y \Upsilon(r), \quad v(x, y, 0) = 15 + \varepsilon x \Upsilon(r), \quad \Upsilon(r) := \begin{cases} 5, & r \leq \dfrac{1}{5}, \\ \dfrac{2}{r} - 5, & \dfrac{1}{5} < r \leq \dfrac{2}{5}, \\ 0, & r \geq \dfrac{2}{5}, \end{cases}$$

where $r := \sqrt{x^2 + y^2}$. These initial data correspond to a rotating vortex traveling along a circular path.

We compute the solution by both the proposed AP and explicit schemes until the final time $T = 0.98$. In Fig. 7, we show the computed trajectories of the traveling vortex center, that is, mesh points $(x_{j_{\min}}(t), y_{k_{\min}}(t))$ at which $\{\overline{h}_{j,k}(t)\}$ achieves its minimum value at time $t \in [0, T]$. As one can see, the captured trajectories are very close to each other.

Fig. 8 shows the contour lines of h computed at the final time $T = 0.98$ by the proposed AP and explicit schemes. It can be observed that the AP scheme preserves the shape of the rotating vortex much better than the explicit scheme. Moreover, in Fig. 9, we show the side view of the simulated traveling vortex. As one can clearly see, the resolution achieved by the AP scheme is much higher as by the final time the initial vortex structure is almost destroyed by the explicit scheme.

5. Conclusion

In the current study, we have developed an AP scheme for the 2-D low-Froude number shallow water system with Coriolis forces. The method is based on splitting the flux into a sum of the nonlinear nonstiff and linear stiff flux terms, which model the slow and fast dynamics, respectively. In order to relax the constraint of the time step due to the stiff terms, an IMEX Runge-Kutta ODE solver is used to evolve the solution in time. To this end, the nonstiff part of the flux is discretized explicitly using a second-order central-upwind approach and the stiff part is resolved by implementing a Poisson solver using an implicit second-order central difference method.

The developed scheme is AP in the sense that it provides consistent and stable approximation of the underlying system in the low Froude number regime, in which both the mesh size and time steps are to be selected based on the accuracy consideration only. Numerical examples presented in the paper clearly demonstrate that the proposed AP scheme yields efficient, accurate and stable approximation for the 2-D Saint-Venant system of shallow water equations with Coriolis forces in all Froude number regimes.
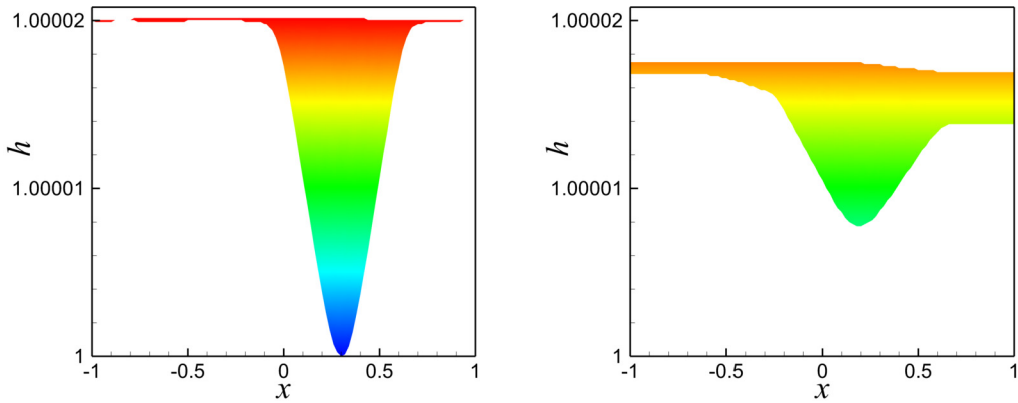
Fig. 9. Example 2: Side view of h computed by the proposed AP (left) and explicit (right) schemes.

Acknowledgements

Appendix A. Implementation of the ARS(2,2,2) scheme

Here, we describe how the temporal accuracy of the AP scheme (3.40)–(3.42) can be increased to the second order using the ARS(2,2,2) method described by the Butcher tableau (3.43). As ARS(2,2,2) is a two-stage IMEX method, we will introduce the $(\cdot)^*$ notation for all of the quantities computed at the first stage.

The first stage of the ARS(2,2,2) method reads as

$$\frac{h^* - h^n}{\Delta t} + \gamma\alpha(hu)_x^n + \gamma\alpha(hv)_y^n + \gamma(1-\alpha)(hu)_x^* + \gamma(1-\alpha)(hv)_y^* = 0, \tag{A.1}$$

$$\frac{(hu)^* - (hu)^n}{\Delta t} + \gamma\left(hu^2 + \frac{\frac{1}{2}h^2 - a^n h}{\varepsilon^2}\right)_x^n + \gamma(huv)_y^n + \frac{\gamma a^n}{\varepsilon^2}h_x^* = \frac{\gamma}{\varepsilon}(hv)^*, \tag{A.2}$$

$$\frac{(hv)^* - (hv)^n}{\Delta t} + \gamma(huv)_x^n + \gamma\left(hv^2 + \frac{\frac{1}{2}h^2 - a^n h}{\varepsilon^2}\right)_y^n + \frac{\gamma a^n}{\varepsilon^2}h_y^* = -\frac{\gamma}{\varepsilon}(hu)^*. \tag{A.3}$$

We note that the system (A.1)–(A.3) coincides with the system (3.17)–(3.19) with Δt replaced with $\tau := \gamma\Delta t$. Therefore, following the same steps as in §3.5, we arrive at

$$\overline{h}_{j,k}^* - \frac{a^n(1-\alpha)}{\widetilde{K}_\tau}\Delta\overline{h}_{j,k}^* = \overline{h}_{j,k}^n + \tau\mathcal{R}_{j,k}^{(h),n}$$

$$- \frac{\tau(1-\alpha)}{K_\tau}\left[D_x\overline{(hu)}_{j,k}^n + D_y\overline{(hv)}_{j,k}^n + \frac{\tau}{\varepsilon}\left(D_x\overline{(hv)}_{j,k}^n - D_y\overline{(hu)}_{j,k}^n\right)\right. \tag{A.4}$$

$$\left. + \tau\left(D_x\mathcal{R}_{j,k}^{(hu),n} + D_y\mathcal{R}_{j,k}^{(hv),n}\right) + \frac{\tau^2}{\varepsilon}\left(D_x\mathcal{R}_{j,k}^{(hv),n} - D_y\mathcal{R}_{j,k}^{(hu),n}\right)\right],$$

$$\overline{(hu)}_{j,k}^* = \frac{1}{K_\tau}\left[\overline{(hu)}_{j,k}^n + \frac{\tau}{\varepsilon}\overline{(hv)}_{j,k}^n + \tau\left(\mathcal{R}_{j,k}^{(hu),n} + \frac{\tau}{\varepsilon}\mathcal{R}_{j,k}^{(hv),n}\right) - \frac{a^n\tau}{\varepsilon^2}\left(D_x\overline{h}_{j,k}^* + \frac{\tau}{\varepsilon}D_y\overline{h}_{j,k}^*\right)\right], \tag{A.5}$$

$$\overline{(hv)}_{j,k}^* = \frac{1}{K_\tau}\left[\overline{(hv)}_{j,k}^n - \frac{\tau}{\varepsilon}\overline{(hu)}_{j,k}^n + \tau\left(\mathcal{R}_{j,k}^{(hv),n} - \frac{\tau}{\varepsilon}\mathcal{R}_{j,k}^{(hu),n}\right) - \frac{a^n\tau}{\varepsilon^2}\left(D_y\overline{h}_{j,k}^* - \frac{\tau}{\varepsilon}D_x\overline{h}_{j,k}^*\right)\right], \tag{A.6}$$

where $K_\tau := 1 + (\tau/\varepsilon)^2$ and $\widetilde{K}_\tau := 1 + (\varepsilon/\tau)^2$.

After finding h^*, $(hu)^*$ and $(hv)^*$ from (A.4)–(A.6), we continue with the second stage of the ARS(2,2,2) method, which reads as

$$\frac{h^{n+1} - h^n}{\Delta t} + \gamma(1-\alpha)\left[(hu)_x^{n+1} + (hv)_y^{n+1}\right] + (1-\gamma)(1-\alpha)\left[(hu)_x^* + (hv)_y^*\right]$$

$$= \frac{1}{2\gamma}R^{(h),*} + \left(1 - \frac{1}{2\gamma}\right)R^{(h),n}, \tag{A.7}$$

$$\frac{(hu)^{n+1} - (hu)^n}{\Delta t} - \frac{\gamma}{\varepsilon}(hv)^{n+1} + \frac{\gamma a^*}{\varepsilon^2}h_x^{n+1} - \frac{(1-\gamma)}{\varepsilon}(hv)^* + \frac{(1-\gamma)a^n}{\varepsilon^2}h_x^*$$
$$= \frac{1}{2\gamma}R^{(hu),*} + \left(1 - \frac{1}{2\gamma}\right)R^{(hu),n}, \tag{A.8}$$

$$\frac{(hv)^{n+1} - (hv)^n}{\Delta t} + \frac{\gamma}{\varepsilon}(hu)^{n+1} + \frac{\gamma a^*}{\varepsilon^2}h_y^{n+1} + \frac{(1-\gamma)}{\varepsilon}(hu)^* + \frac{(1-\gamma)a^n}{\varepsilon^2}h_y^*$$
$$= \frac{1}{2\gamma}R^{(hv),*} + \left(1 - \frac{1}{2\gamma}\right)R^{(hv),n}. \tag{A.9}$$

We solve (A.7)–(A.9) for h^{n+1}, $(hu)^{n+1}$ and $(hv)^{n+1}$ to obtain

$$h^{n+1} = h^n - \tau(1-\alpha)\left[(hu)_x^{n+1} + (hv)_y^{n+1}\right] - (\Delta t - \tau)(1-\alpha)\left[(hu)_x^* + (hv)_y^*\right]$$
$$+ \frac{\Delta t}{2\gamma}R^{(h),*} + \left(1 - \frac{1}{2\gamma}\right)\Delta t R^{(h),n}, \tag{A.10}$$

$$(hu)^{n+1} = \frac{1}{K_\tau}\left[(hu)^n + \frac{\tau}{\varepsilon}(hv)^n + \frac{\Delta t}{2\gamma}\left\{R^{(hu),*} + \frac{\tau}{\varepsilon}R^{(hv),*}\right\} + \left(1 - \frac{1}{2\gamma}\right)\Delta t\left\{R^{(hu),n} + \frac{\tau}{\varepsilon}R^{(hv),n}\right\}\right.$$
$$\left. + \frac{\Delta t - \tau}{\varepsilon}\left((hv)^* - \frac{\tau}{\varepsilon}(hu)^*\right) - \frac{a^*\tau}{\varepsilon^2}\left(h_x^{n+1} + \frac{\tau}{\varepsilon}h_y^{n+1}\right) - \frac{a^n(\Delta t - \tau)}{\varepsilon^2}\left(h_x^* + \frac{\tau}{\varepsilon}h_y^*\right)\right], \tag{A.11}$$

$$(hv)^{n+1} = \frac{1}{K_\tau}\left[(hv)^n - \frac{\tau}{\varepsilon}(hu)^n + \frac{\Delta t}{2\gamma}\left\{R^{(hv),*} - \frac{\tau}{\varepsilon}R^{(hu),*}\right\} + \left(1 - \frac{1}{2\gamma}\right)\Delta t\left\{R^{(hv),n} - \frac{\tau}{\varepsilon}R^{(hu),n}\right\}\right.$$
$$\left. - \frac{\Delta t - \tau}{\varepsilon}\left((hu)^* + \frac{\tau}{\varepsilon}(hv)^*\right) - \frac{a^*\tau}{\varepsilon^2}\left(h_y^{n+1} - \frac{\tau}{\varepsilon}h_x^{n+1}\right) - \frac{a^n(\Delta t - \tau)}{\varepsilon^2}\left(h_y^* - \frac{\tau}{\varepsilon}h_x^*\right)\right]. \tag{A.12}$$

We then differentiate equations (A.11) and (A.12) with respect to x and y, respectively, substitute them into equation (A.10) and obtain the following elliptic equation for h^{n+1}:

$$h^{n+1} - \frac{a^*(1-\alpha)}{\widetilde{K}_\tau}\left(h_{xx}^{n+1} + h_{yy}^{n+1}\right) = h^n + \left(1 - \frac{1}{2\gamma}\right)\Delta t R^{(h),n} + \frac{\Delta t}{2\gamma}R^{(h),*}$$
$$- \frac{\tau(1-\alpha)}{K_\tau}\left[(hu)_x^n + (hv)_y^n + \frac{\tau}{\varepsilon}\left((hv)_x^n - (hu)_y^n\right)\right.$$
$$+ \left(1 - \frac{1}{2\gamma}\right)\Delta t\left\{R_x^{(hu),n} + R_y^{(hv),n} + \frac{\tau}{\varepsilon}\left(R_x^{(hv),n} - R_y^{(hu),n}\right)\right\} \tag{A.13}$$
$$+ \frac{\Delta t - \tau}{\varepsilon}\left\{(hv)_x^* - (hu)_y^* - \frac{\tau}{\varepsilon}(1 - \widetilde{K}_\tau)\left((hu)_x^* + (hv)_y^*\right)\right\}$$
$$+ \frac{\Delta t}{2\gamma}\left\{R_x^{(hu),*} + R_y^{(hv),*} + \frac{\tau}{\varepsilon}\left(R_x^{(hv),*} - R_y^{(hu),*}\right)\right\} - \frac{a^n(\Delta t - \tau)}{\varepsilon^2}\left(h_{xx}^* + h_{yy}^*\right)\right].$$

We then compute the nonstiff flux terms $R^{(h),n}$, $R^{(hu),n}$, $R^{(hv),n}$, $R^{(h),*}$, $R^{(hu),*}$ and $R^{(hv),*}$ using the central-upwind flux approximation from §3.4 and discretize all of the spatial derivatives in (A.13) using the standard second-order central differences. This results in

$$\overline{h}_{j,k}^{n+1} - \frac{a^*(1-\alpha)}{\widetilde{K}_\tau}\Delta\overline{h}_{j,k}^{n+1} = \overline{h}_{j,k}^n + \left(1 - \frac{1}{2\gamma}\right)\Delta t \mathcal{R}_{j,k}^{(h),n} + \frac{\Delta t}{2\gamma}\mathcal{R}_{j,k}^{(h),*}$$
$$- \frac{\tau(1-\alpha)}{K_\tau}\left[D_x\overline{(hu)}_{j,k}^n + D_y\overline{(hv)}_{j,k}^n + \frac{\tau}{\varepsilon}\left(D_x\overline{(hv)}_{j,k}^n - D_y\overline{(hu)}_{j,k}^n\right)\right.$$
$$+ \left(1 - \frac{1}{2\gamma}\right)\Delta t\left\{\left(D_x\mathcal{R}_{j,k}^{(hu),n} + D_y\mathcal{R}_{j,k}^{(hv),n}\right) + \frac{\tau}{\varepsilon}\left(D_x\mathcal{R}_{j,k}^{(hv),n} - D_y\mathcal{R}_{j,k}^{(hu),n}\right)\right\} \tag{A.14}$$
$$+ \frac{\Delta t - \tau}{\varepsilon}\left\{\left(D_x\overline{(hv)}_{j,k}^* - D_y\overline{(hu)}_{j,k}^*\right) - \frac{\tau}{\varepsilon}(1 - \widetilde{K}_\tau)\left(D_x\overline{(hu)}_{j,k}^* + D_y\overline{(hv)}_{j,k}^*\right)\right\}$$
$$+ \frac{\Delta t}{2\gamma}\left\{\left(D_x\mathcal{R}_{j,k}^{(hu),*} + D_y\mathcal{R}_{j,k}^{(hv),*}\right) + \frac{\tau}{\varepsilon}\left(D_x\mathcal{R}_{j,k}^{(hv),*} - D_y\mathcal{R}_{j,k}^{(hu),*}\right)\right\} - \frac{a^n(\Delta t - \tau)}{\varepsilon^2}\Delta\overline{h}_{j,k}^*\right].$$

After solving the linear algebra system (A.14) for $\{\overline{h}_{j,k}^{n+1}\}$, we substitute it into equations (A.11) and (A.12) discretized using the standard central differences and end up with

$$\overline{(hu)}_{j,k}^{n+1} = \frac{1}{K_\tau}\left[\overline{(hu)}_{j,k}^{n} + \frac{\Delta t}{\varepsilon}\overline{(hv)}_{j,k}^{n} + \frac{\Delta t}{2\gamma}\left(\mathcal{R}_{j,k}^{(hu),*} + \frac{\tau}{\varepsilon}\mathcal{R}_{j,k}^{(hv),*}\right)\right.$$
$$+ \left(1 - \frac{1}{2\gamma}\right)\Delta t\left(\mathcal{R}_{j,k}^{(hu),n} + \frac{\tau}{\varepsilon}\mathcal{R}_{j,k}^{(hv),n}\right) + \frac{\Delta t - \tau}{\varepsilon}\left(\overline{(hv)}_{j,k}^{*} - \frac{\tau}{\varepsilon}\overline{(hu)}_{j,k}^{*}\right)$$
$$\left. - \frac{a^*\tau}{\varepsilon^2}\left(D_x\overline{h}_{j,k}^{n+1} + \frac{\tau}{\varepsilon}D_y\overline{h}_{j,k}^{n+1}\right) - \frac{a^n(\Delta t - \tau)}{\varepsilon^2}\left(D_x\overline{h}_{j,k}^{*} + \frac{\tau}{\varepsilon}D_y\overline{h}_{j,k}^{*}\right)\right],$$

$$\overline{(hv)}_{j,k}^{n+1} = \frac{1}{K_\tau}\left[\overline{(hv)}_{j,k}^{n} - \frac{\Delta t}{\varepsilon}\overline{(hu)}_{j,k}^{n} + \frac{\Delta t}{2\gamma}\left(\mathcal{R}_{j,k}^{(hv),*} - \frac{\tau}{\varepsilon}\mathcal{R}_{j,k}^{(hu),*}\right)\right.$$
$$+ \left(1 - \frac{1}{2\gamma}\right)\Delta t\left(\mathcal{R}_{j,k}^{(hv),n} - \frac{\tau}{\varepsilon}\mathcal{R}_{j,k}^{(hu),n}\right) - \frac{\Delta t - \tau}{\varepsilon}\left(\overline{(hu)}_{j,k}^{*} + \frac{\tau}{\varepsilon}\overline{(hv)}_{j,k}^{*}\right)$$
$$\left. - \frac{a^*\tau}{\varepsilon^2}\left(D_y\overline{h}_{j,k}^{n+1} - \frac{\tau}{\varepsilon}D_x\overline{h}_{j,k}^{n+1}\right) - \frac{a^n(\Delta t - \tau)}{\varepsilon^2}\left(D_y\overline{h}_{j,k}^{*} - \frac{\tau}{\varepsilon}D_x\overline{h}_{j,k}^{*}\right)\right].$$

References

[1] U.M. Ascher, S.J. Ruuth, R.J. Spiteri, Implicit-explicit Runge-Kutta methods for time-dependent partial differential equations, Appl. Numer. Math. 25 (1997) 151–167.
[2] E. Audusse, R. Klein, D.D. Nguyen, S. Vater, Preservation of the discrete geostrophic equilibrium in shallow water flows, in: Finite Volumes for Complex Applications VI Problems & Perspectives, in: Springer Proceedings in Mathematics, vol. 4, Springer, Berlin Heidelberg, 2011, pp. 59–67.
[3] E. Audusse, R. Klein, A. Owinoh, Conservative discretization of Coriolis force in a finite volume framework, J. Comput. Phys. 228 (2009) 2934–2950.
[4] G. Bispen, K.R. Arun, M. Lukáčová-Medviďová, S. Noelle, IMEX large time step finite volume methods for low Froude number shallow water flows, Commun. Comput. Phys. 16 (2014) 307–347.
[5] G. Bispen, M. Lukáčová-Medviďová, L. Yelash, Asymptotic preserving IMEX finite volume schemes for low Mach number Euler equations with gravitation, J. Comput. Phys. 335 (2017) 222–248.
[6] F. Bouchut, J. Le Sommer, V. Zeitlin, Frontal geostrophic adjustment and nonlinear wave phenomena in one-dimensional rotating shallow water. II. High-resolution numerical simulations, J. Fluid Mech. 514 (2004) 35–63.
[7] A. Chertock, M. Dudzinski, A. Kurganov, M. Lukáčová-Medviďová, Well-balanced schemes for the shallow water equations with Coriolis forces, Numer. Math. 138 (2018) 939–973.
[8] F. Cordier, P. Degond, A. Kumbaro, An asymptotic-preserving all-speed scheme for the Euler and Navier-Stokes equations, J. Comput. Phys. 231 (2012) 5685–5704.
[9] P. Degond, M. Tang, All speed scheme for the low Mach number limit of the isentropic Euler equations, Commun. Comput. Phys. 10 (2011) 1–31.
[10] G. Dimarco, R. Loubère, M.-H. Vignal, Study of a new asymptotic preserving scheme for the Euler system in the low Mach number limit, SIAM J. Sci. Comput. 39 (2017) A2099–A2128.
[11] A. Duran, F. Marche, R. Turpault, C. Berthon, Asymptotic preserving scheme for the shallow water equations with source terms on unstructured meshes, J. Comput. Phys. 287 (2015) 184–206.
[12] H. Guillard, A. Murrone, On the behavior of upwind schemes in the low Mach number limit: II. Godunov type schemes, Comput. Fluids 33 (2004) 655–675.
[13] H. Guillard, C. Viozat, On the behaviour of upwind schemes in the low Mach number limit, Comput. Fluids 28 (1999) 63–86.
[14] J. Haack, S. Jin, J.-G. Liu, An all-speed asymptotic-preserving method for the isentropic Euler and Navier-Stokes equations, Commun. Comput. Phys. 12 (2012) 955–980.
[15] A. Harten, P. Lax, B. van Leer, On upstream differencing and Godunov-type schemes for hyperbolic conservation laws, SIAM Rev. 25 (1983) 35–61.
[16] J. Hu, S. Jin, Q. Li, Asymptotic-preserving schemes for multiscale hyperbolic and kinetic equations, in: Handbook of Numerical Methods for Hyperbolic Problems, in: Handb. Numer. Anal., vol. 18, Elsevier/North-Holland, Amsterdam, 2017, pp. 103–129.
[17] S. Jin, Runge-Kutta methods for hyperbolic conservation laws with stiff relaxation terms, J. Comput. Phys. 122 (1995) 51–67.
[18] S. Jin, Efficient asymptotic-preserving (AP) schemes for some multiscale kinetic equations, SIAM J. Sci. Comput. 21 (1999) 441–454, (electronic).
[19] S. Jin, Asymptotic preserving (ap) schemes for multiscale kinetic and hyperbolic equations: a review, Riv. Mat. Univ. Parma 3 (2012) 177–2016.
[20] S. Jin, L. Pareschi, G. Toscani, Uniformly accurate diffusive relaxation schemes for multiscale transport equations, SIAM J. Numer. Anal. 38 (2000) 913–936.
[21] R. Klein, Semi-implicit extension of a Godunov-type scheme based on low Mach number asymptotics, I: one-dimensional flow, J. Comput. Phys. 121 (1995) 213–237.
[22] R. Klein, E. Mikusky, A. Owinoh, Multiple scales asymptotics for atmospheric flows, in: European Congress of Mathematics, Eur. Math. Soc., Zürich, 2005, pp. 201–220.
[23] A. Kurganov, Central schemes: a powerful black-box solver for nonlinear hyperbolic PDEs, in: Handbook of Numerical Methods for Hyperbolic Problems, in: Handb. Numer. Anal., vol. 17, Elsevier/North-Holland, Amsterdam, 2016, pp. 525–548.
[24] A. Kurganov, C.-T. Lin, On the reduction of numerical dissipation in central-upwind schemes, Commun. Comput. Phys. 2 (2007) 141–163.
[25] A. Kurganov, S. Noelle, G. Petrova, Semi-discrete central-upwind scheme for hyperbolic conservation laws and Hamilton-Jacobi equations, SIAM J. Sci. Comput. 23 (2001) 707–740.
[26] A. Kurganov, E. Tadmor, Solution of two-dimensional Riemann problems for gas dynamics without Riemann problem solvers, Numer. Methods Partial Differ. Equ. 18 (2002) 584–608.
[27] K.-A. Lie, S. Noelle, On the artificial compression method for second-order nonoscillatory central difference schemes for systems of conservation laws, SIAM J. Sci. Comput. 24 (2003) 1157–1174.
[28] H. Nessyahu, E. Tadmor, Nonoscillatory central differencing for hyperbolic conservation laws, J. Comput. Phys. 87 (1990) 408–463.
[29] S. Noelle, G. Bispen, K.R. Arun, M. Lukáčová-Medviďová, C.-D. Munz, A weakly asymptotic preserving low Mach number scheme for the Euler equations of gas dynamics, SIAM J. Sci. Comput. 36 (2014) B989–B1024.
[30] F. Rieper, On the dissipation mechanism of upwind-schemes in the low Mach number regime: a comparison between Roe and HLL, J. Comput. Phys. 229 (2010) 221–232.
[31] P.K. Sweby, High resolution schemes using flux limiters for hyperbolic conservation laws, SIAM J. Numer. Anal. 21 (1984) 995–1011.

[32] B. van Leer, Towards the ultimate conservative difference scheme. V. A second-order sequel to Godunov's method, J. Comput. Phys. 32 (1979) 101–136.
[33] S. Vater, R. Klein, A semi-implicit multiscale scheme for shallow water flows at low Froude number, Commun. Appl. Math. Comput. Sci. 13 (2018) 303–336.
[34] H. Zakerzadeh, The RS-IMEX scheme for the rotating shallow water equations with the Coriolis force, in: Finite Volumes for Complex Applications VIII—Hyperbolic, Elliptic and Parabolic Problems, in: Springer Proc. Math. Stat., vol. 200, Springer, Cham, 2017, pp. 199–207.
[35] V. Zeitlin, Geophysical Fluid Dynamics: Understanding (almost) Everything with Rotating Shallow Water Models, Oxford University Press, Oxford, 2018.